Measurement of antineutrino scattering on free protons in MINERνA

Tejin Cai

University of Rochester
York University

Fermilab Colloquium,
Feb 1, 2023

High resolution image of Andromeda galaxy

Credit:NASA, ESA, J. Dalcanton (University of Washington, USA), B. F. Williams (University of Washington, USA), L. C. Johnson (University of Washington, USA), the PHAT team, and R. Gendler.

Hale Bopp, visible in 1997,
photo by E. Kolmhofer, H. Raab,
Johannes-Kepler-Observatory/ Wikimedia Commons

Comet C/2022 E3 (ZTF), photo by Steven Bellavia. Should be visible today!

Neutrinos are interesting because ...

Super-K and SNO confirmed neutrino oscillate in 1998 and 2001. Neutrinos are produced in one of the three flavor eigenstates: e, μ, τ, but travels as a mixture of mass eigenstates:

$$|\nu_\alpha\rangle = \sum_i U^*_{\alpha i} |\nu_{\mathbf{i}}\rangle$$

with the PMNS mixing matrix U:

$$\begin{bmatrix} \nu_e \\ \nu_\mu \\ \nu_\tau \end{bmatrix} = \begin{pmatrix} 1 & 0 & 0 \\ 0 & c_{23} & s_{23} \\ 0 & -s_{23} & c_{23} \end{pmatrix} \begin{pmatrix} c_{13} & 0 & e^{-i\delta_{\mathrm{CP}}} s_{13} \\ 0 & 1 & 0 \\ -e^{i\delta_{\mathrm{CP}}} s_{13} & 0 & c_{13} \end{pmatrix} \begin{pmatrix} c_{12} & s_{12} & 0 \\ -s_{12} & c_{12} & 0 \\ 0 & 0 & 1 \end{pmatrix} \begin{bmatrix} \nu_1 \\ \nu_2 \\ \nu_3 \end{bmatrix}$$

where $c_{ij} = \cos\theta_{ij}$, $s_{ij} = \sin\theta_{ij}$, and δ_{CP} is the CP-violating phase.

Neutrinos are interesting because ...

Super-K and SNO confirmed neutrino oscillate in 1998 and 2001. Neutrinos are produced in one of the three flavor eigenstates: e, μ, τ, but travels as a mixture of mass eigenstates:

$$|\nu_\alpha\rangle = \sum_i U^*_{\alpha i} |\nu_i\rangle$$

$$\begin{aligned}
|\nu_j(t)\rangle &= e^{-i(E_j t - \vec{p}\vec{x})}|\nu_j(0)\rangle \\
&\approx e^{-i\left(\frac{m_j^2 L}{2E}\right)}|\nu_j(0)\rangle \\
P_{\alpha\to\beta} &= \langle\nu_\beta|\nu_\alpha\rangle \\
&= \delta_{\alpha\beta} - 4\sum \mathcal{R}(U_{\alpha i}U^*_{\beta i}U^*_{\alpha j}U_{\beta j})\sin^2\left(\frac{\Delta m^2_{ij} L}{4E}\right) + \ldots
\end{aligned}$$

L: Distance
E: Energy
$\Delta m^2_{ij} = m^2_i - m^2_j$

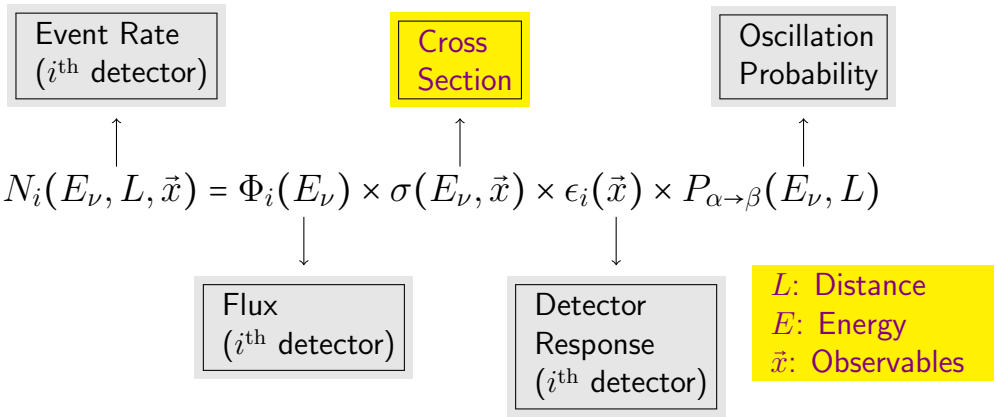

- Near/far detector scheme means potentially different Φ and ϵ.
- Systematics do not fully cancel.
- σ contains nucleon and nuclear physics. Difficult to model.

An active areas of research ...

Important for oscillation measurements

Physics of neutrino cross sections

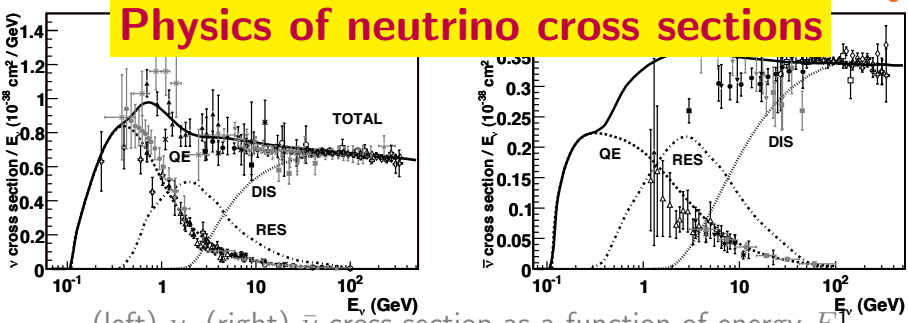

(left) ν, (right) $\bar{\nu}$ cross section as a function of energy E[1]

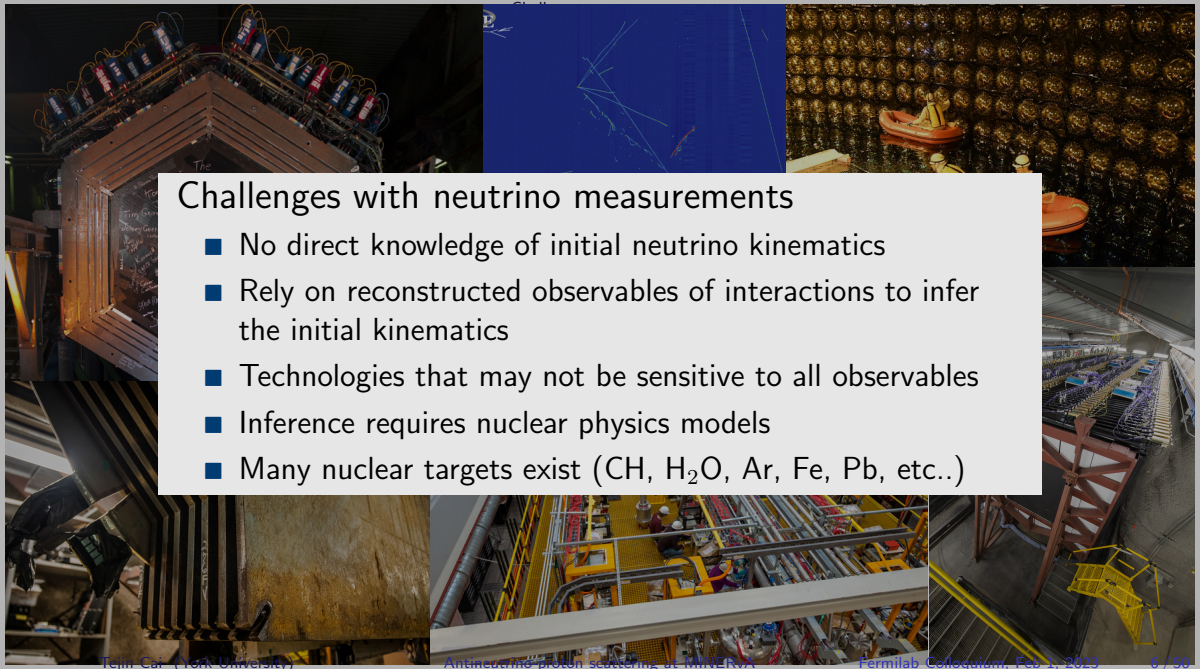

Challenges with neutrino measurements

- No direct knowledge of initial neutrino kinematics
- Rely on reconstructed observables of interactions to infer the initial kinematics
- Technologies that may not be sensitive to all observables
- Inference requires nuclear physics models
- Many nuclear targets exist (CH, H_2O, Ar, Fe, Pb, etc..)

Difficulty: No direct knowledge of the neutrino kinematics

- Neutrinos are neutral – do not ionize atoms
- Energy and momentum reconstruction depends on
  - visible calorimetric energy and/or
  - final state particle kinematics
- Don't see everything – need models.

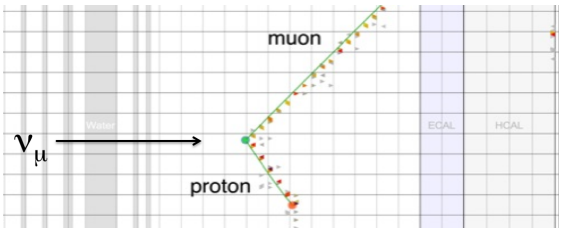

Figure: MINERvA event display, a muon and a proton in the final states

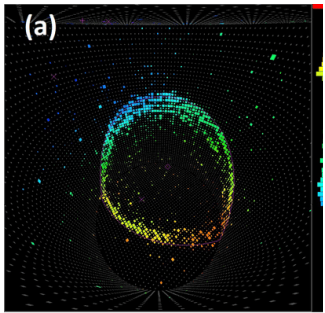

Figure: A muon-like ring in Super-K

MINERνA

Main **I**njector **N**eutrino **E**xpe**R**iment ν-**A** studies neutrino-nucleus scatterings at the few-GeV region:

- Precise measurements of the signal and background processes relevant to oscillation experiments.
- Improves understanding of nuclear effects that affect the reconstruction of neutrino energy.
- Demonstrates experimental techniques that benefit current and future oscillation experiments.

Nucleon and nuclear physics

Free nucleon (proton or neutron) response to charged current (CC) interactions

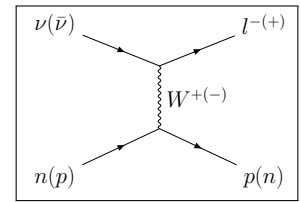

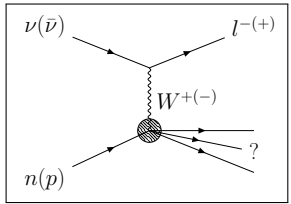

Folding in nuclear effects from multiple bound nucleons

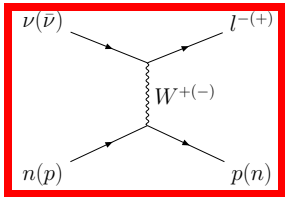

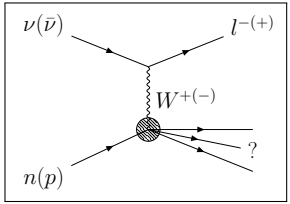

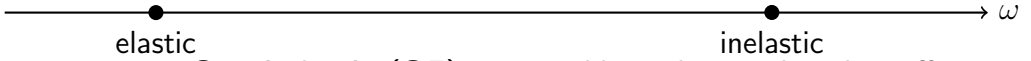

Quasi-elastic (QE): inseparable nucleon and nuclear effects.

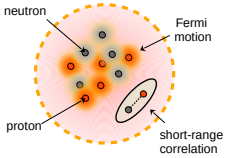

Initial States:
Fermi motion
short-range correlation
binding energy, etc.

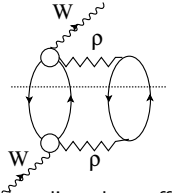

2p2h/mutli-nucleon effects

Final State Interactions (FSI):
elastic, inelastic, charge-exchange,pion production, pion absorption, etc.

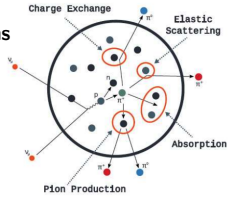

Quasi-elastic-like (QELike): only nucleons in the final states.

Nucleon physics

Form factors parameterize QCD processes.

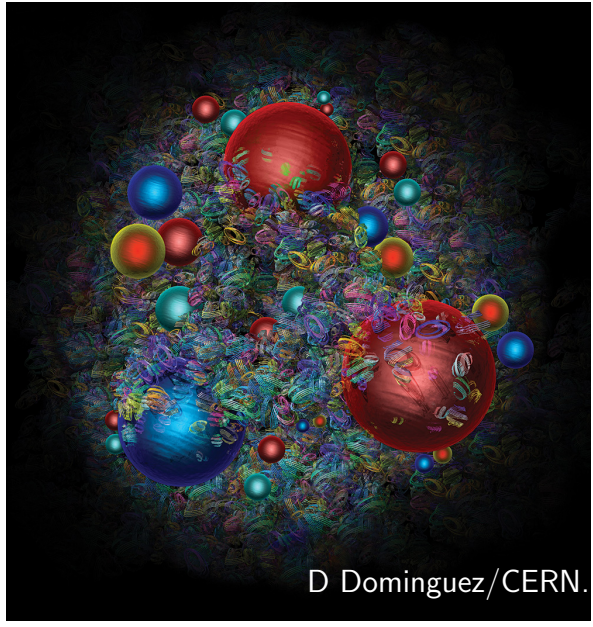

Nucleon physics

Form factors parameterize QCD processes.

Low 4-momentum squared (Q^2): Fourier transform of charge distribution $\sim$ charge radius as $Q^2 \to 0$.

i.e. exponential charge distribution $\to$ dipole form factor F^D

Experiments can access **much higher** Q^2 $\to$ more theory guidance needed appreciated!

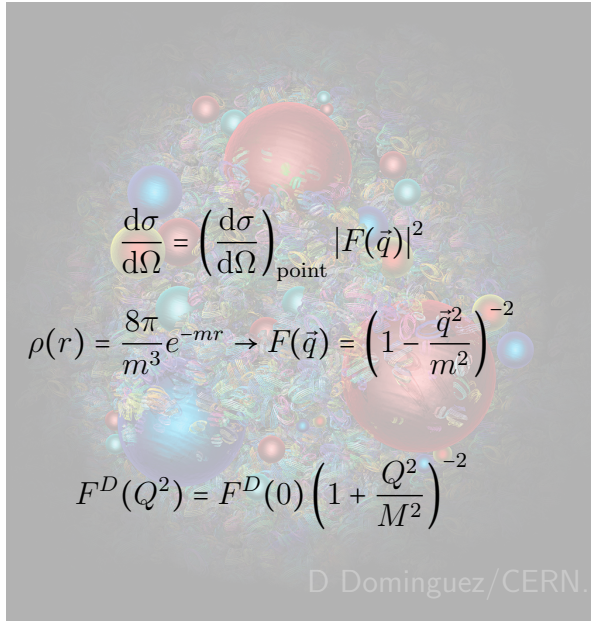

Free nucleon cross section: Llewllyn Smith, 1971[2]

$$\frac{\mathrm{d}\sigma}{\mathrm{d}Q^2}\begin{pmatrix}\nu n \to l^- p \\ \bar{\nu} p \to l^+ n\end{pmatrix} = \frac{M^2 G_\mathrm{F}^2 \cos^2\theta_c}{8\pi E_\nu^2}\left[A(Q^2) \mp B(Q^2)\frac{(s-u)}{M^2} + C(Q^2)\frac{(s-u)^2}{M^4}\right], \tag{1}$$

$$\begin{aligned}
A(Q^2) &= \frac{m^2+Q^2}{4M^2}\left[\left(4+\frac{Q^2}{M^2}\right)|F_\mathrm{A}|^2 - \left(4-\frac{Q^2}{M^2}\right)|F_\mathrm{V}^1|^2\right. \\
&\quad \left. + \frac{Q^2}{M^2}\left(1-\frac{Q^2}{4M^2}\right)|\xi F_\mathrm{V}^2|^2 + \frac{4Q^2}{M^2}\mathrm{Re}F_\mathrm{V}^{1*}\xi F_\mathrm{V}^2 + \mathcal{O}\left(\frac{m^2}{M^2}\right)\right], \\
B(Q^2) &= \frac{Q^2}{M^2}\mathrm{Re}F_\mathrm{A}^*(F_\mathrm{V}^1 + \xi F_\mathrm{V}^2), \\
C(Q^2) &= \frac{1}{4}\left(|F_\mathrm{A}|^2 + |F_\mathrm{V}^1|^2 + \frac{Q^2}{4M^2}|\xi F_\mathrm{V}^2|^2\right)
\end{aligned} \tag{2}$$

Depends on the "form factors", F_V^1, ξF_V^2, and F_A.

Free nucleon cross section: Llewllyn Smith, 1971[2]

$$\frac{\mathrm{d}\sigma}{\mathrm{d}Q^2}\begin{pmatrix}\nu n \to l^- p\\ \bar{\nu} p \to l^+ n\end{pmatrix} = \frac{M^2 G_\mathrm{F}^2 \cos^2\theta_c}{8\pi E_\nu^2}\left[A(Q^2) \mp B(Q^2)\frac{(s-u)}{M^2} + C(Q^2)\frac{(s-u)^2}{M^4}\right], \tag{1}$$

$$\begin{aligned}
A(Q^2) &= \frac{m^2+Q^2}{4M^2}\left[\left(4+\frac{Q^2}{M^2}\right)|F_\mathrm{A}|^2 - \left(4-\frac{Q^2}{M^2}\right)|F_\mathrm{V}^1|^2\right.\\
&\quad \left. + \frac{Q^2}{M^2}\left(1-\frac{Q^2}{4M^2}\right)|\xi F_\mathrm{V}^2|^2 + \frac{4Q^2}{M^2}\mathrm{Re}F_\mathrm{V}^{1*}\xi F_\mathrm{V}^2 + \mathcal{O}\left(\frac{m^2}{M^2}\right)\right],\\
B(Q^2) &= \frac{Q^2}{M^2}\mathrm{Re}F_\mathrm{A}^*(F_\mathrm{V}^1 + \xi F_\mathrm{V}^2),\\
C(Q^2) &= \frac{1}{4}\left(|F_\mathrm{A}|^2 + |F_\mathrm{V}^1|^2 + \frac{Q^2}{4M^2}|\xi F_\mathrm{V}^2|^2\right)
\end{aligned} \tag{2}$$

Depends on the "form factors", F_V^1, ξF_V^2, and F_A.

Neutrino-nucleon cross section depends on

- F_{V}^1, ξF_{V}^2: electric and magnetic charge, measured by electron scattering experiments – lots of data.
- F_{A}: axial vector "charge". Accessible only through neutrino scattering – very little data exists.
  - likelihood of $u \leftrightarrow d$ conversion.
  - Historically assumed a dipole form:

$$F_{\mathrm{A}}(Q^2) = F_{\mathrm{A}}(0)\left(1 + \frac{Q^2}{M_A^2}\right)^{-2}$$

  - $F_{\mathrm{A}}(0) = -1.2723 \pm 0.0023$ from neutron decay measurements[3].
  - M_A is the axial mass.

$D_2(H)$ bubble chambers

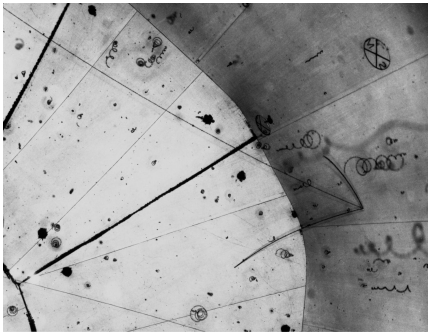

First neutrino detected by ANL 12-ft D2 bubble chamber.

Past bubble chamber experiments (ANL 12-ft, BNL 7-ft, FNAL 15-ft, 1973-1983) primarily measured $\nu D \to \mu^- + p + p^S$ reactions.
BNL measured $\bar{\nu} H$ reaction using 13 events.

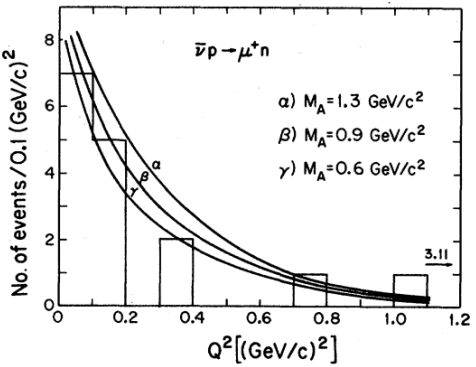

$\bar{\nu} - H$

Fanourakis et al., 1980[4]

Mann et al., 1973[5]

First neutrino - deuterium measurement

Reported exactly 50 years ago:

- Flux uncertainty was 15%
- Extracting form factor needs model-dependent deuterium corrections
  - Fermi motion
  - Pauli exclusion principle

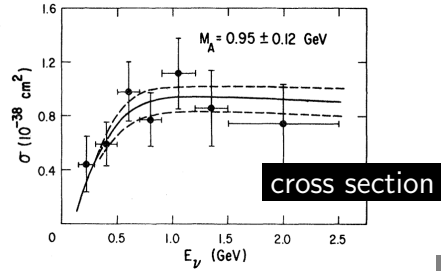

$\nu - D$

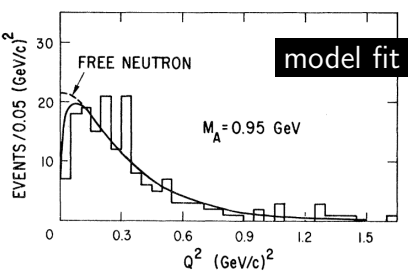

Measurements with heavier targets

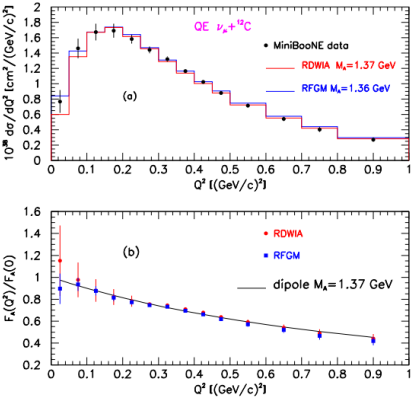

MiniBooNE QE measurement
Aguilar-Arevalo et al., 2010[6]
Butkevich and Perevalov, 2013[7]

- MiniBooNE – inclusive, lepton-only measurement – interpreted as F_{A} on carbon, insensitive to lepton-hadron correlation.

Measurements with heavier targets

MINERνA ν_μ QE measurement

Fiorentini et al.,2013[8]

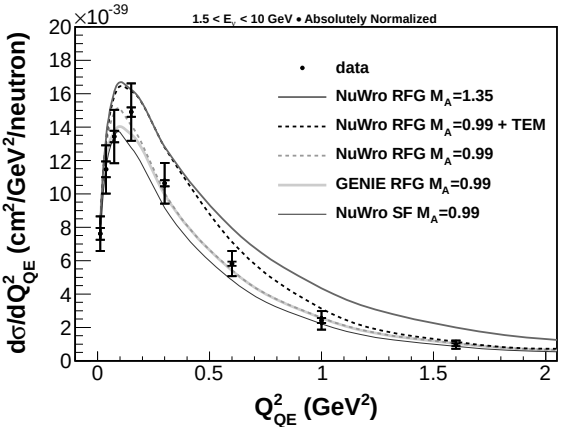

- MiniBooNE – inclusive, lepton-only measurement – interpreted as F_A on carbon, insensitive to lepton-hadron correlation.
- MINERνA QE results: disagree with $M_A = 1.35\ \mathrm{GeV}/c^2$
  - Tension points to nuclear effects.

Measurements with heavier targets

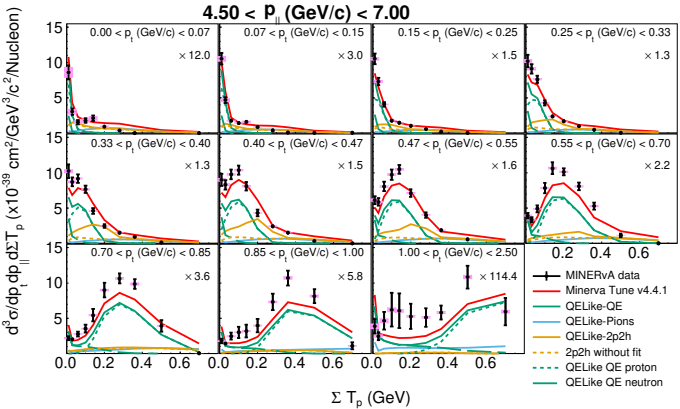

Muon $p_{\parallel}$ vs muon p_t vs total proton kinetic energy
MINERνA Ruterbories et al., 2022[9]

- MiniBooNE – inclusive, lepton-only measurement – interpreted as F_A on carbon, insensitive to lepton-hadron correlation.
- MINERνA QE results: disagree with $M_A = 1.35\ \mathrm{GeV}/c^2$
  - Tension points to nuclear effects.
- Better able to identify nuclear effects with lepton-hadron correlations.

Nucleon and nuclear effects are inseparable

Neutrino measurements depend on models.
Most factor out nucleon and nuclear effects:

1. Neutrino-nucleon interactions
2. Fermi motion, binding energy
3. Final state interactions
4. Event kinematics → combine uncertainty from previous steps!

NEUT

A model-independent nucleon F_{A} measurement is beneficial

How – in the future we could build a new bubble chamber.

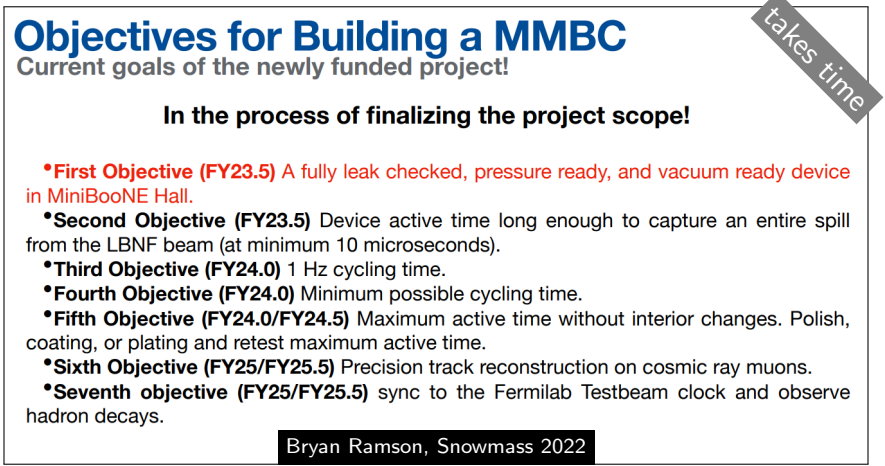

How – could perform C/CH ratio

Fractional uncertainty for C/CH ratio in MINERνA

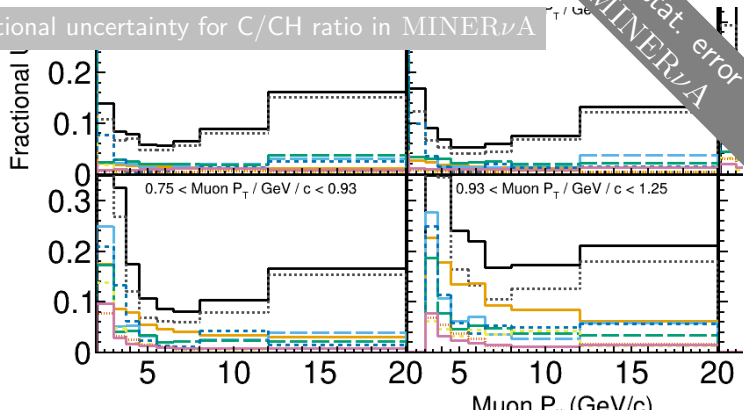

MINERνA nuclear target measurement with neutrinos, Kleykamp et al., 2023[10]

How – could perform C/CH ratio

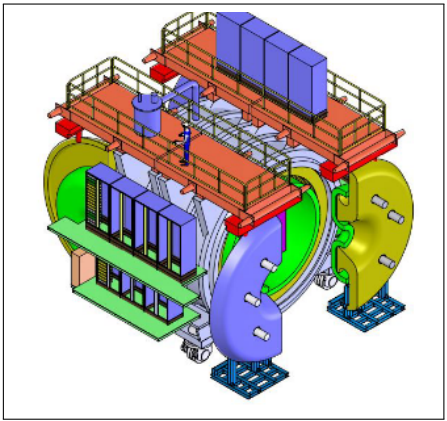

Figure from Vicenzi, 2022[11]

DUNE's near detector SAND is planning a C/CH ratio measurement in the next decade.

How – directly measure H from a CH target!

Measure the charged current elastic (CCE) scattering

$$\bar{\nu}_\mu + p \to \mu^+ + n,$$

with the Medium Energy NuMI antineutrino beam, and the scintillators in MINERνA.

- No nuclear effect on hydrogen.
- Large carbon background.

Extracting the cross section – a road map

$$\left(\frac{\mathrm{d}\sigma}{\mathrm{d}Q^2}\right)_i = \frac{\sum_j U_{ji}\left(N_j^{\mathrm{data}} - N_j^{\mathrm{bkg-pred}}\right)}{\Phi T \epsilon_i \left(\Delta Q^2\right)_i}$$

Extracting the cross section – a road map

$$\left(\frac{\mathrm{d}\sigma}{\mathrm{d}\mathbf{Q^2}}\right)_{\mathbf{i}} = \frac{\sum_j U_{ji}\left(N_j^{\mathrm{data}} - N_j^{\mathrm{bkg-pred}}\right)}{\Phi T \epsilon_i (\mathbf{\Delta Q^2})_{\mathbf{i}}}$$

- Q^2: square of the 4-momentum transfer.
- Reconstructed quantity:
  - $E_{\bar{\nu}} = \frac{M_{\mathrm{n}}^2 - M_{\mathrm{p}}^2 - m_\mu^2 + 2M_{\mathrm{p}}E_\mu}{2(M_{\mathrm{p}} - E_\mu + p_\mu \cos\theta_\mu)}$
  - $Q^2_{\mathrm{QE}} = 2E_{\bar{\nu}}(E_\mu - p_\mu \cos\theta_\mu) - m_\mu^2$
- $(d\sigma/dQ^2)_i$: cross section in the i^{th} Q^2 bin.
- $(\Delta Q^2)_i$: width of the i^{th} bin.

Extracting the cross section – a road map

$$\left(\frac{\mathrm{d}\sigma}{\mathrm{d}Q^2}\right)_i = \frac{\sum_j \mathbf{U_{ji}}\left(N_j^{\mathrm{data}} - N_j^{\mathrm{bkg-pred}}\right)}{\mathbf{\Phi T}\epsilon_{\mathbf{i}}(\Delta Q^2)_i}$$

- U_{ji}: Unfolding matrix – correcting detector smearing.
- Φ: (Anti)neutrino flux (Zazueta et al., 2022[12]).
- T: Number of hydrogen atoms in the sinctillator.
- ϵ_i: Detector efficiency in the i^{th} bin.

Extracting the cross section – a road map

$$\left(\frac{\mathrm{d}\sigma}{\mathrm{d}Q^2}\right)_i = \frac{\sum_j U_{ji}\left(\mathbf{N_j^{data}} - \mathbf{N_j^{bkg-pred}}\right)}{\Phi T \epsilon_i (\Delta Q^2)_i}$$

- Measured Q^2_{QE}:
  - N_j^{data}: detected event rate in the j^{th} Q^2_{QE} bin.
  - $N_j^{\mathrm{bkg-pred}}$: reconstructed background prediction in the same bin.
- Everything sounds simple, except
  - signal channel is not dominant, and
  - background channels are not necessarily well-modeled.

Needs to get clever with data selection!

Using nuclear effects to advantage

$\bar{\nu}_\mu H$ is a 2-body process.
Real, elastic, flavor-changing, billiard balls. We know exactly where the neutron would go.

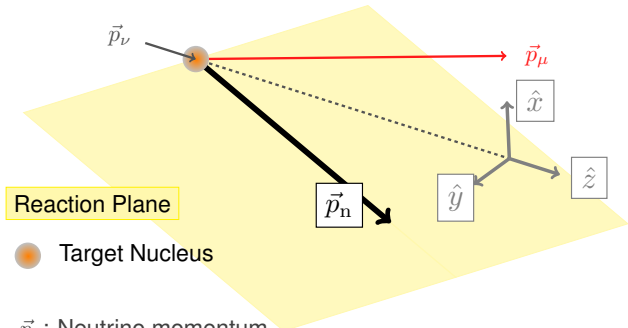

Using nuclear effects to advantage

$\bar{\nu}_\mu H$ is a 2-body process.
Real, elastic, flavor-changing, billiard balls. We know exactly where the neutron would go.

Carbon doesn't play by the same rules. Neutrons happily deviate.

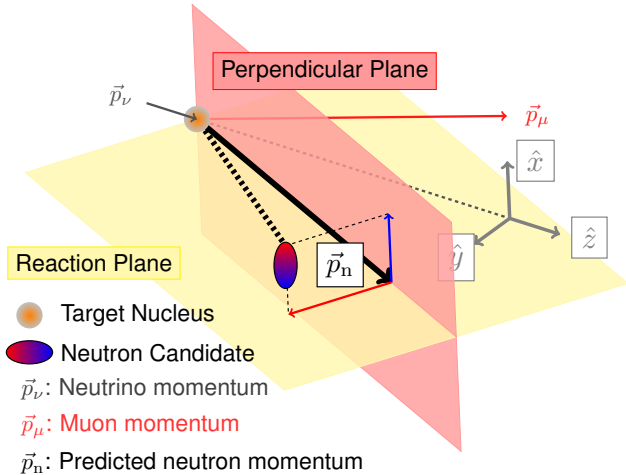

Using nuclear effects to advantage

$\bar{\nu}_\mu H$ is a 2-body process. Real, elastic, flavor-changing, billiard balls. We know exactly where the neutron would go.

Carbon doesn't play by the same rules. Neutrons happily deviate.

Capture this deviation in neutron direction, using $\delta\theta_{\mathrm{P}}$ and $\delta\theta_{\mathrm{R}}$

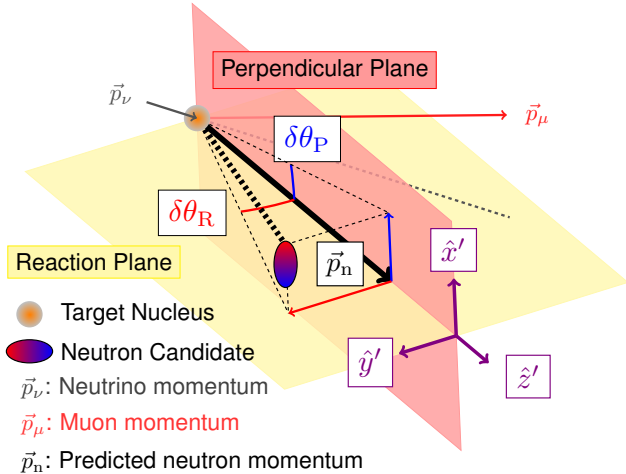

Wait, you need neutrons?

MINERνA detector

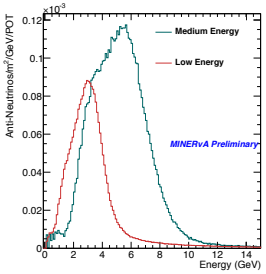

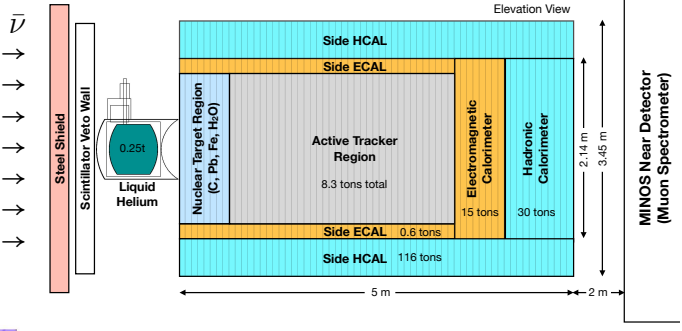

Nucl. Inst. and Meth. A743 (2014) 130.

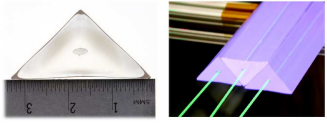

Element	# of Targets
H	2.61×10^{29}
C	2.38×10^{29}

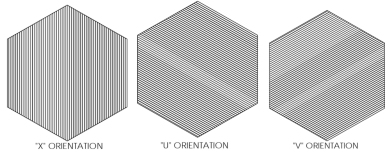

Neutrons inside the detector interact with hydrogen or carbon to produce charged secondary particles.

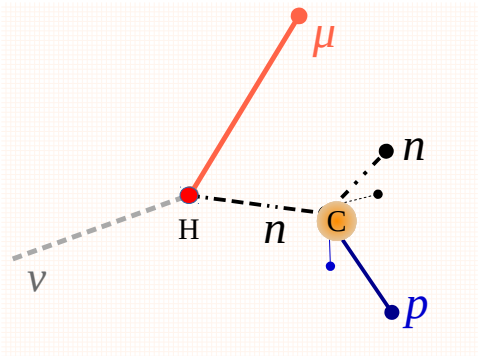

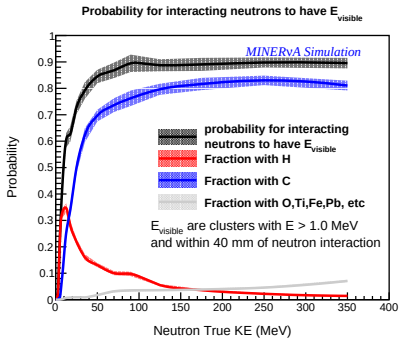

Most prompt neutron energy deposits due to knockout protons.

Neutron signature

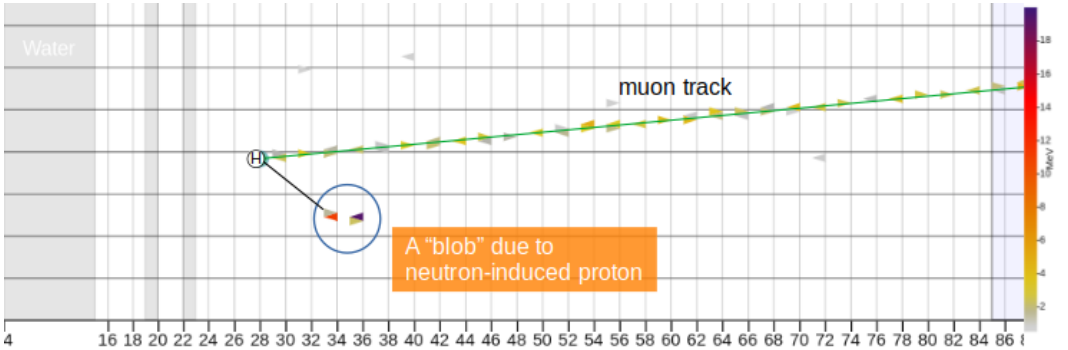

An incoming anti-neutrino scatters off a hydrogen producing neutron. The neutron undergoes secondary interactions to produce visible proton.

Blobbing algorithm

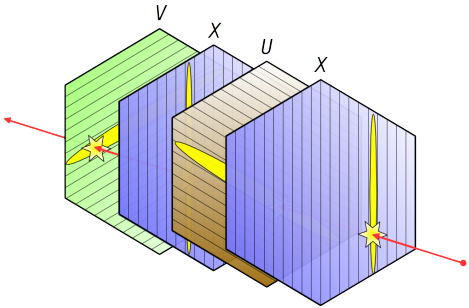

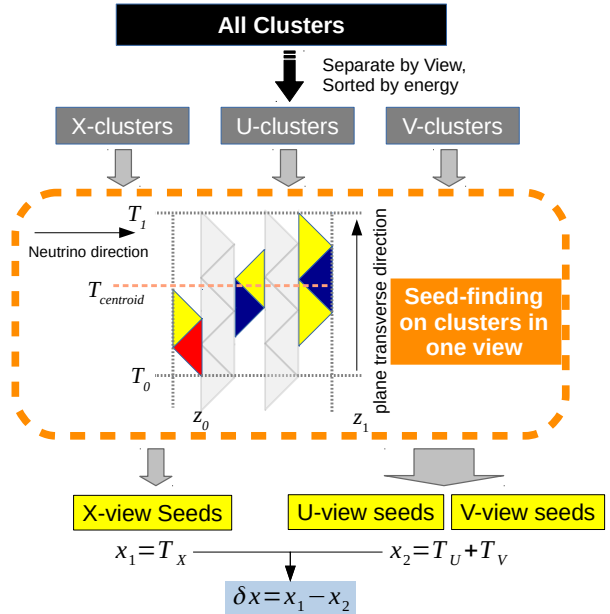

Blobbing algorithm

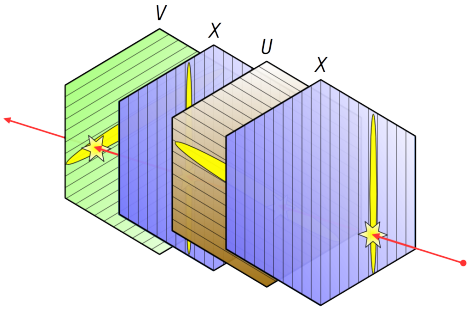

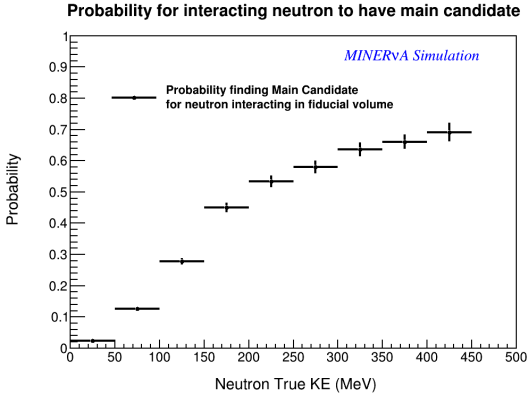

Forming event selection

Event topology:

- 1 μ^+ and no reconstructed hadronic track

Neutron selection:

- ≥ 1 three-dimensional neutron candidate
- Leading candidate energy deposited $10\ \mathrm{cm}$ away from the muon axis.

Muon acceptance due to detector shape:

- $1.5\ \mathrm{GeV} < E_\mu < 20\ \mathrm{GeV}$
- $\theta_\mu < 20^\circ$ w.r.t. to neutrino beam

NuMI Antineutrino Mode: 1.12×10^{21} Protons on Target

Total recoil energy cut:

Condition	$E_{\mathrm{max}}^{\mathrm{recoil}}$ (GeV)
$Q^2_{\mathrm{QE}} < 0.3\ (\mathrm{GeV}/c)^2$	$0.04 + 0.43 Q^2_{\mathrm{QE}}/(\mathrm{GeV}/c)^2$
$Q^2_{\mathrm{QE}} < 1.4\ (\mathrm{GeV}/c)^2$	$0.08 + 0.3 Q^2_{\mathrm{QE}}/(\mathrm{GeV}/c)^2$
$Q^2_{\mathrm{QE}} > 1.4\ (\mathrm{GeV}/c)^2$	0.50

A sneak peak at the fun part

~ $94,000$ events.

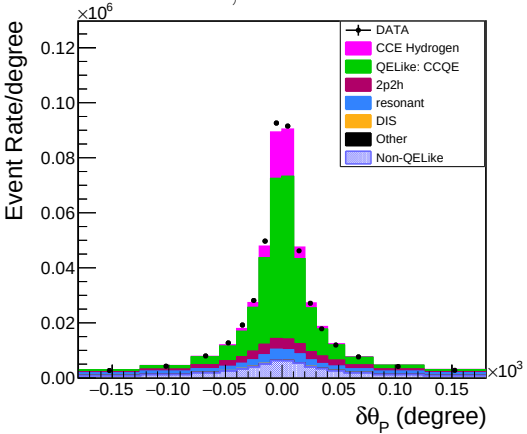

Nuclear effects are real, physics works!

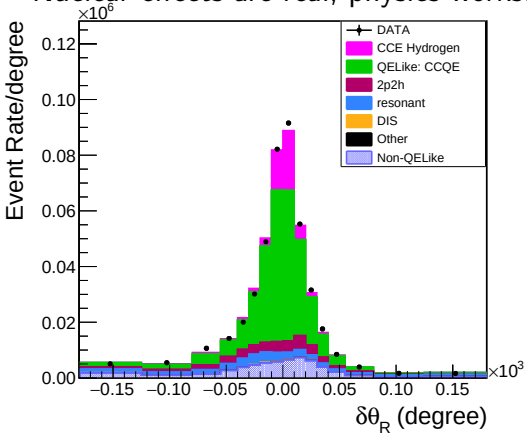

CCE hydrogen QELike CCQE carbon 2p2h

Model prediction

MnvGENIE-v2.5.1

1. Nieves 2p2h[13] and low-recoil tune[14]
2. Random phase approximation[15] (RPA) tune
3. Non-resonant pion reduction[16]
4. Low-Q^2 resonant pion suppression[17]
5. Carbon elastic FSI reweight[18]
6. CCQE carbon NuWro spectral function (SF)[19,20] reweight on GENIE

A GEANT4 neutron reweight[21,22]

Model prediction

MnvGENIE-v2.5.1

1. Nieves 2p2h[13] and low-recoil tune[14]
2. Random phase approximation[15] (RPA) tune
3. Non-resonant pion reduction[16]
4. Low-Q^2 resonant pion suppression[17]
5. Carbon elastic FSI reweight[18]
6. CCQE carbon NuWro spectral function (SF)[19,20] reweight on GENIE

A GEANT4 neutron reweight[21,22]

Rationale for reweighting GENIE relativistic Fermi gas (RFG) model to NuWro's spectral function (SF) model.

Low energy era measurement: MINERνA developed a set of *transverse kinematics imbalance* techniques for the neutrino sample:

- Events with only a primary muon, at least one proton, and no mesons.
- Compare momentum imbalance between μ and p.
- δp_{Ty} measures whether $\vec{p}^{\,\mu} + \vec{p}^{\,\mathrm{p}}$ balance out along the $\vec{p}^{\,\mu}_T$ axis.

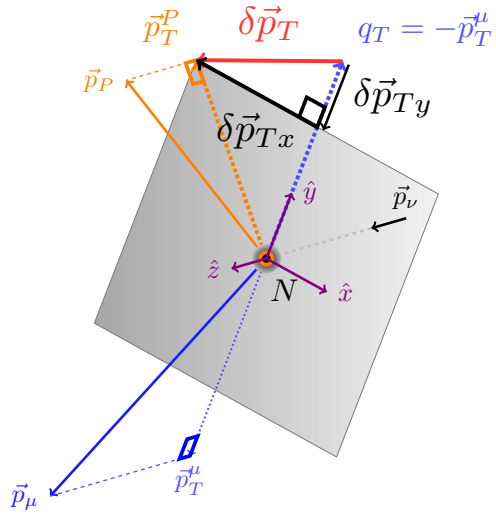

Cai et al., 2019[23]

Low energy era measurement: MINERνA developed a set of *transverse kinematics imbalance* techniques for the neutrino sample:

- Events with only a primary muon, at least one proton, and no mesons.
- Compare momentum imbalance between μ and p.
- δp_{Ty} measures whether $\vec{p}^{\,\mu} + \vec{p}^{\,\mathrm{p}}$ balance out along the $\vec{p}^{\,\mu}_T$ axis.
- NuWro spectral function (solid blue) better describes data.

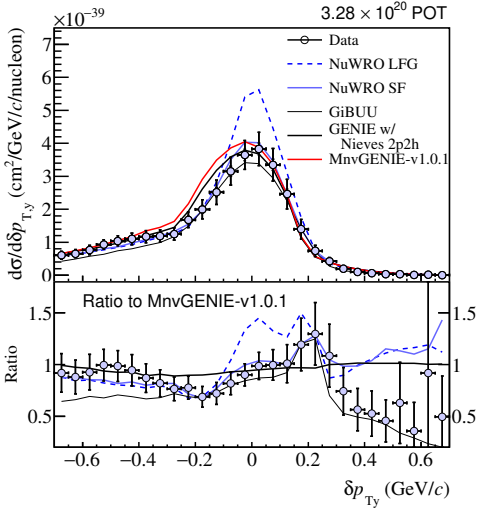

Cai et al., 2019[23]

Constraining $\mathrm{MINER}\nu\mathrm{A}$'s GEANT4 neutron model with external data.

Plot from reference[22]

Neutron model from Modular Neutron Array (MoNA)

- The MoNA collaboration collected (Del Guerra, 1976[21]) and modeled (Kohley et al., 2012[22]) neutron cross section on CH.
- $^{12}C(n, np)^{11}B$ the dominant interaction channel
- We tune each channel to the MoNA cross sections based on secondary daughter particles.

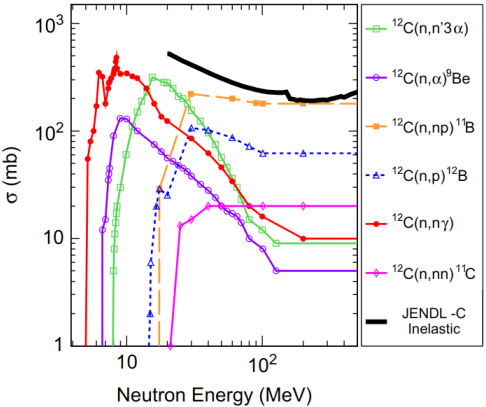

Fig. 3. Inelastic neutron–carbon reaction cross-sections are shown as a function of the incident neutron energy. MENATE_R uses the six different discrete reaction channel cross-sections while the G4-Physics uses the total inelastic reaction cross-sections taken from the JENDL-HE library [37].

- We looked at "nuisance" variables to see if the MONA data improved the data/MC agreement
- These variables are not used in the fit and not tuned
- Example includes energy of neutron candidates, and distance of the candidate to vertex
- will show neutron candidate energy deposits in each Q^2_{QE} bin.

Neutron candidate energy deposits vs Q^2_{QE}
Without MoNA.

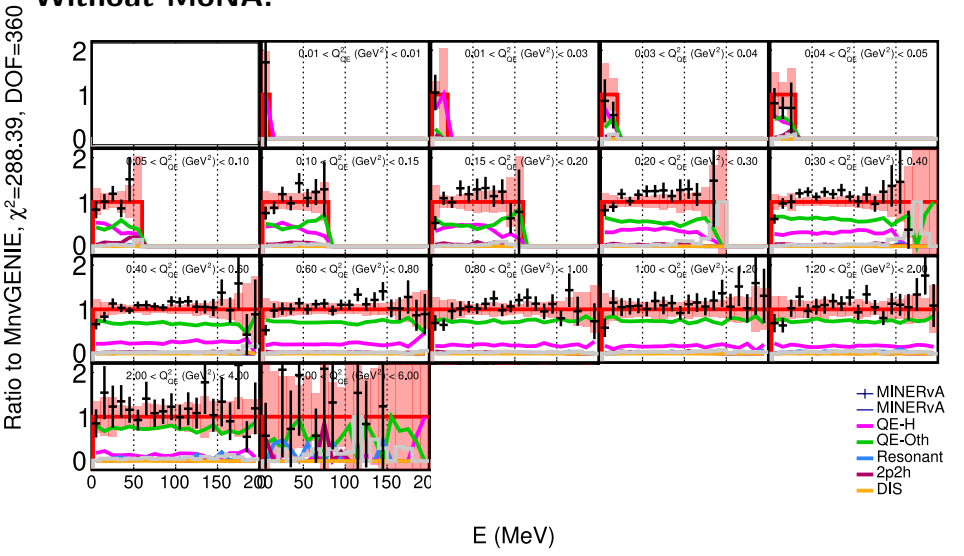

Neutron candidate energy deposits vs Q^2_{QE}

With MoNA: improved χ^2.

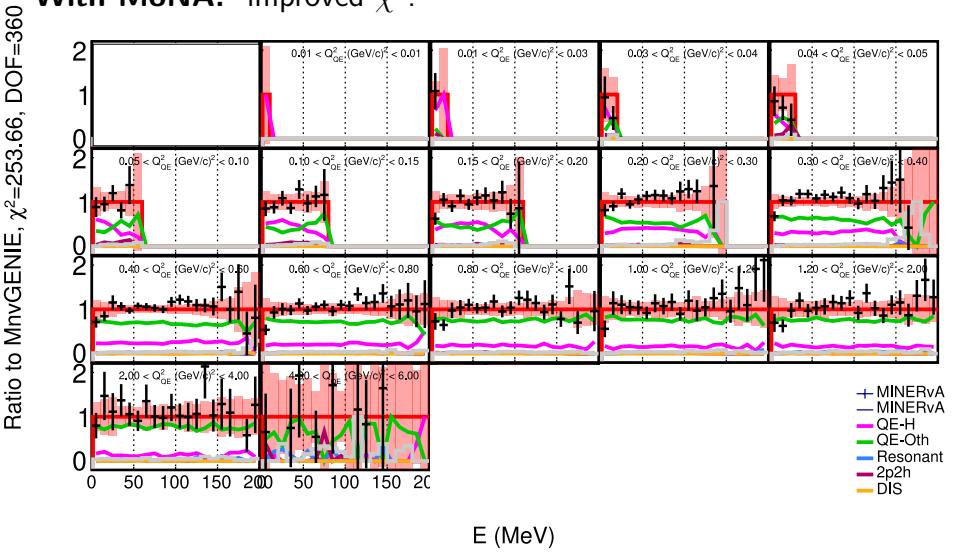

Let's return to the fun part

$\sim 94,000$ events.

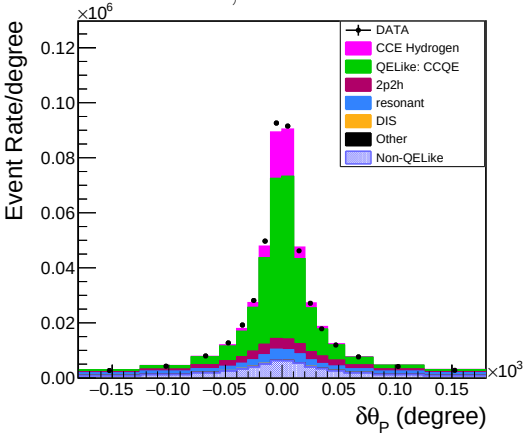

Each angular variable is not selective enough → go to two dimensions

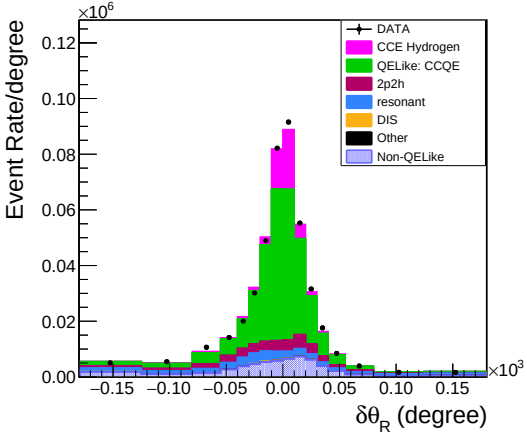

CCE hydrogen | QELike CCQE carbon | 2p2h

Angular regions and MC fraction

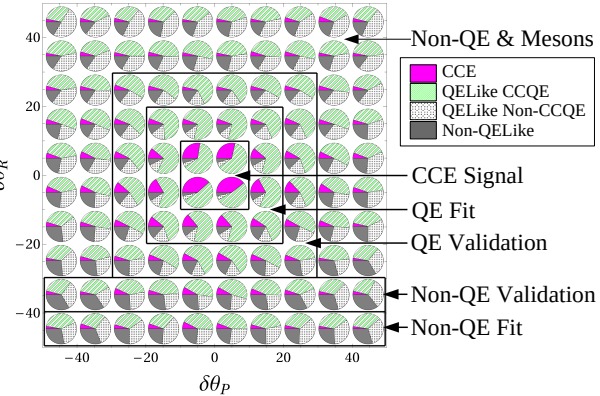

Total data event rate

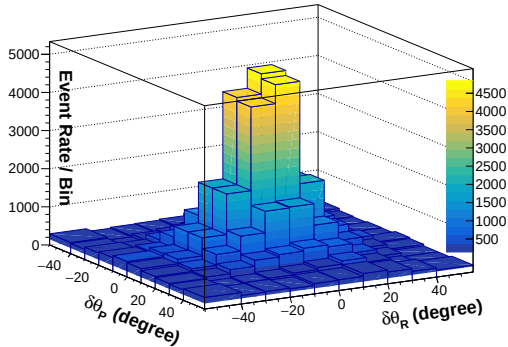

Created different angular regions – Hydrogen signal in the center. Outer regions are used for fit and validation – expand each region in Q^2

Angular regions and MC fraction

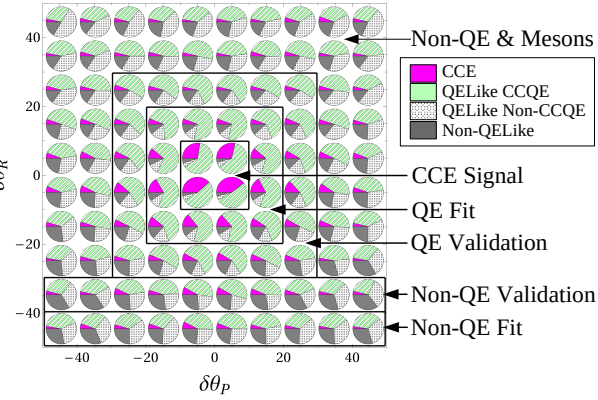

MC events in slices of Q^2

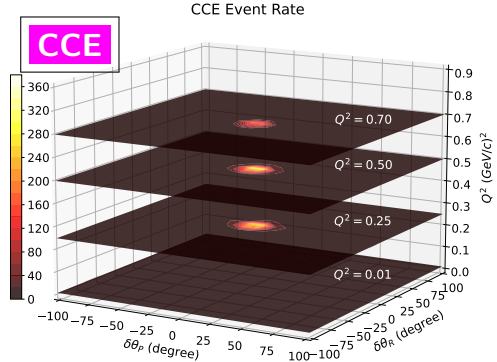

Predicted hydrogen angles – concentrated in the center.

Angular regions and MC fraction

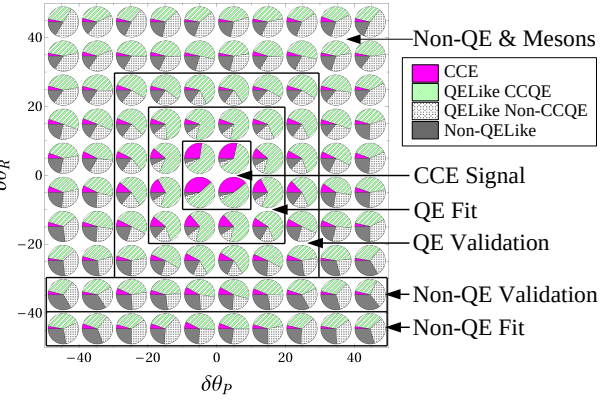

MC events in slices of Q^2

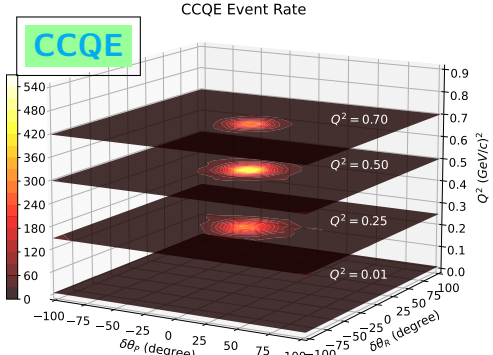

Carbon QELike (CCQE) – more spread out due to Fermi motion and final state interactions.

Angular regions and MC fraction

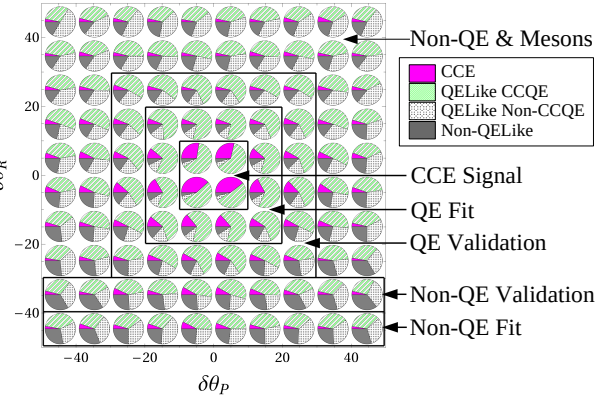

MC events in slices of Q^2

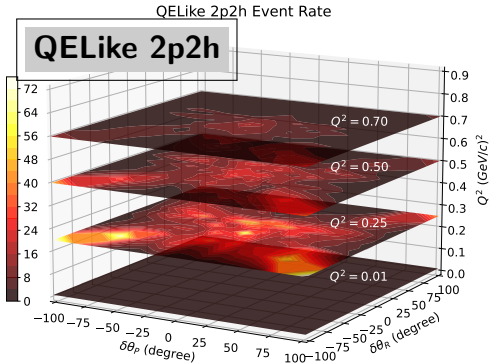

2p2h and resonant – all over the place but different.

Angular regions and MC fraction

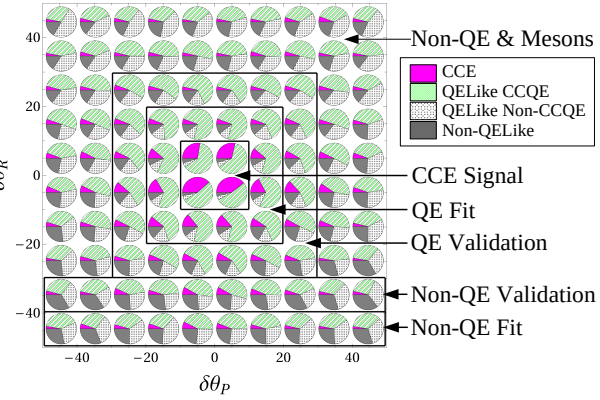

MC events in slices of Q^2

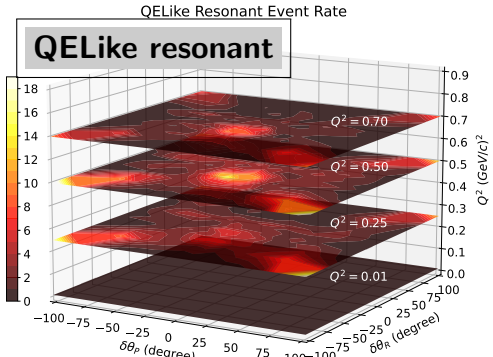

2p2h and resonant – all over the place but different.

Validating background constraint method with neutrino sample

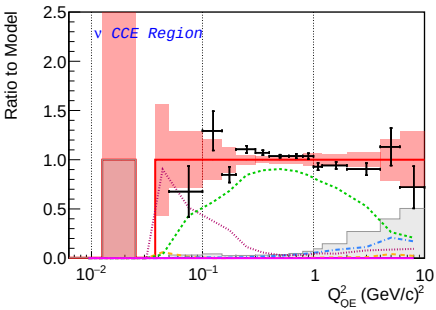

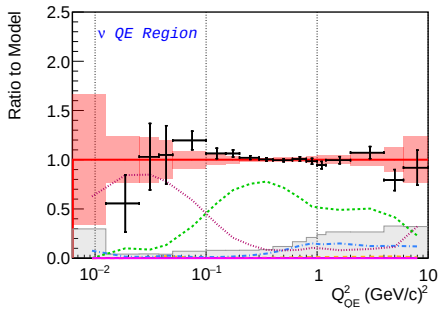

We select events with trackable protons in a **neutrino sample**. Different final states and available kinematics. Apply same fitting mechanism. Data and MC agree within uncertainty except $Q^2 \in (0.2, 0.4)(\mathrm{GeV}/c)^2$.

Validating background constraint method with neutrino sample

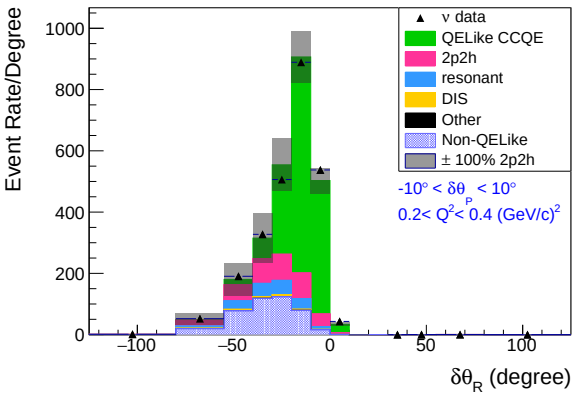

Neutrino mode:

- 100% 2p2h uncertainty covers data/simulation discrepancy.

Antineutrino mode:

- Small 2p2h contribution.
- Sufficiently covered by total uncertainty.

Fit using sideband region

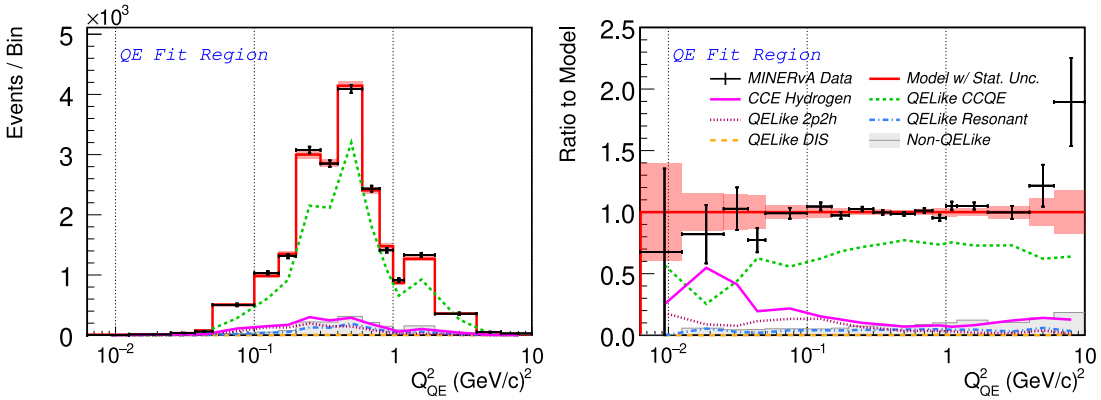

CCQE is the dominant background. Small 2p2h, resonant, and Non-QELike contributions. The fitted model are well constrained by data.

Check fit with validation region

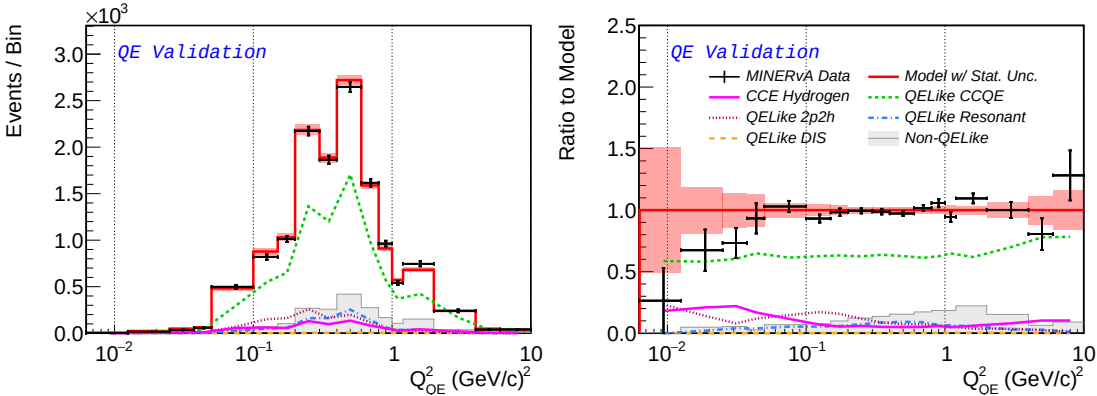

CCQE is the dominant background. Small 2p2h, resonant, and Non-QELike contributions. The fitted model are well constrained by data.

Apply fit to signal region

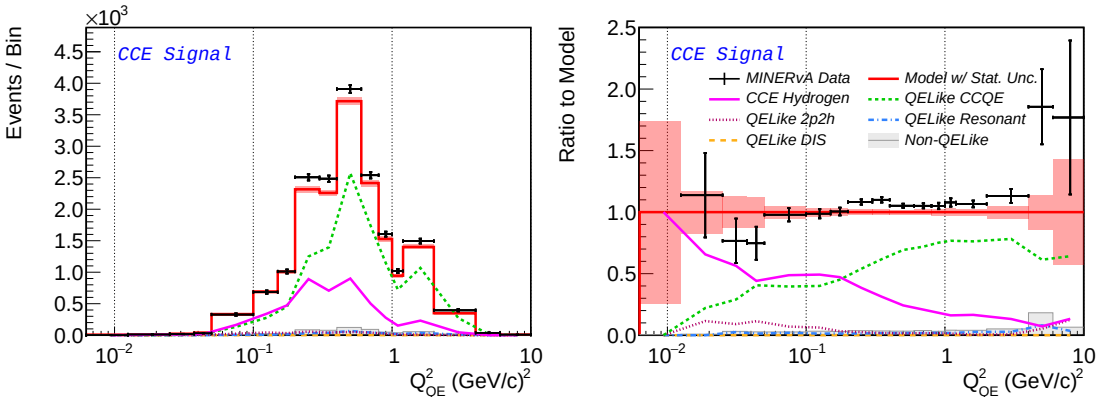

Projecting the fit into the signal region. Difference between data and background is the physics. More than 5000 hydrogen events!

Apply fit to signal region

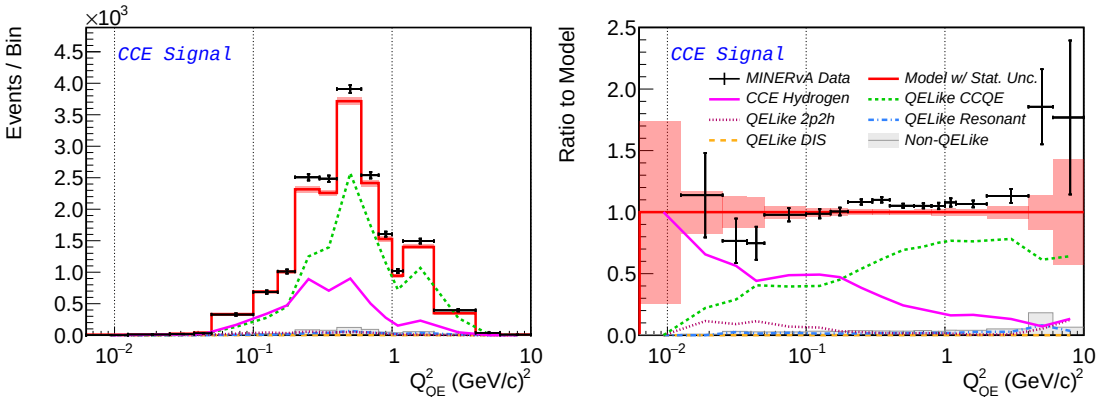

Subtract background, and correct detector smearing using D'Agostini iterative unfolding with 4 iterations.

Efficiency

$$\epsilon = \frac{\texttt{signal events recorded}}{\texttt{total signal events produced}}$$

- Peaks at $Q^2 \sim 0.3\ (\mathrm{GeV}/c)^2$
- Low Q^2: Low acceptance because neutron needs to produce protons that span at least 2 planes.
- high Q^2: Reconstruction inefficiency and larger opening angles and less detector material to contain neutrons.

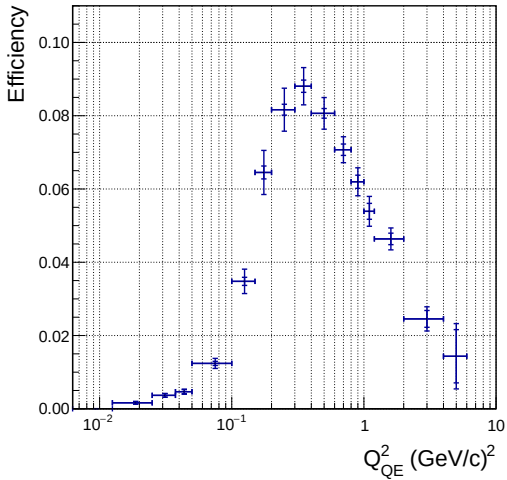

Cross section prediction

- The single nucleon Llewelyn Smith equation convolutes with flux and muon acceptance.
  - Necessary for theory calculations.
- We use a standard vector form factor parameterization. (BBBA2005, Bradford et al., 2005[24])
- F_A fit assumes z-expansion form[25] (details in the backup).

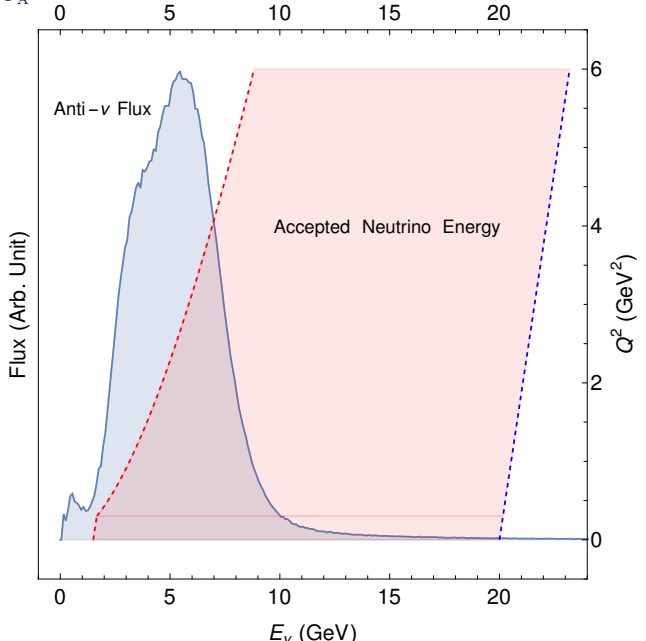

Cross section

Deuterium Fit: Meyer et al., 2016[25]

BBBA2007: Bodek et al. 2007[26]

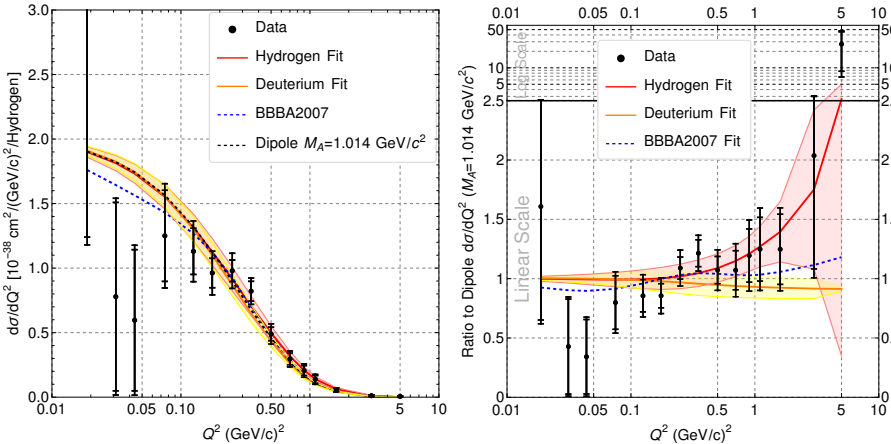

Figure: Extracted cross section and ratio to a dipole form factor.

Systematic and statistical uncertainty

- Dominated by statistical uncertainty from background subtraction, despite enhanced signal
- Systematic uncertainties from residuals of background subtraction
- Particle responses in the "other" category, dominated by neutron systematics.

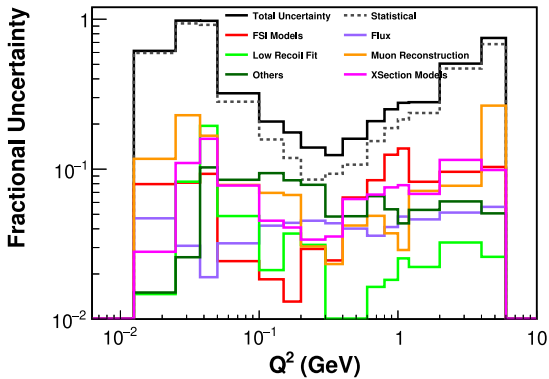

F_A fit and axial radius of the nucleon

LQCD: Lin 2022[27]

Result of F_A fit:

Calculate proton radius from F_A for $Q^2 \to 0$.

$$F_A(Q^2) = F_A(0)\left(1 - \frac{\langle r_A^2\rangle}{3!}Q^2 + \frac{\langle r_A^4\rangle}{5!}Q^4 + \dots\right),$$

$$\frac{1}{F_A(0)}\frac{dF_A}{dQ^2}\bigg|_{Q^2=0} = -\frac{1}{6}\langle r_A{}^2\rangle$$

- $\langle r_A^2\rangle = 0.53(25)\text{fm}^2$
- $\sqrt{\langle r_A^2\rangle} = 0.73(17)\text{fm}$

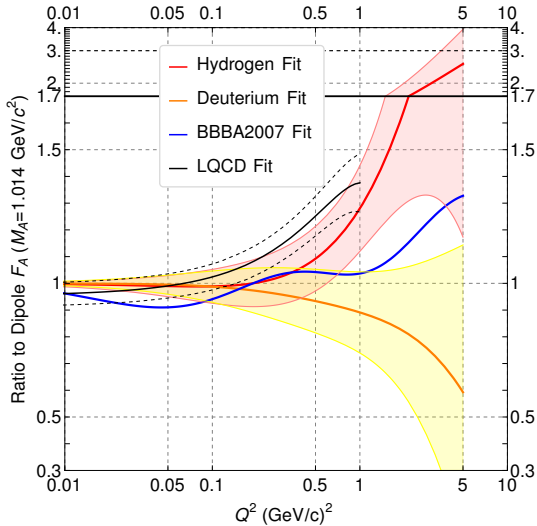

LQCD: Lin 2022[27]

F_A fit and axial radius of the nucleon

Result of F_A fit:

Deuterium fit applies z-expansion to bubble chamber data focused for $Q^2 < 1\ (\mathrm{GeV}/c)^2$.
Hydrogen fit data up to $Q^2 = 5\ (\mathrm{GeV}/c)^2$.
Tension between hydrogen and deuterium at larger Q^2.

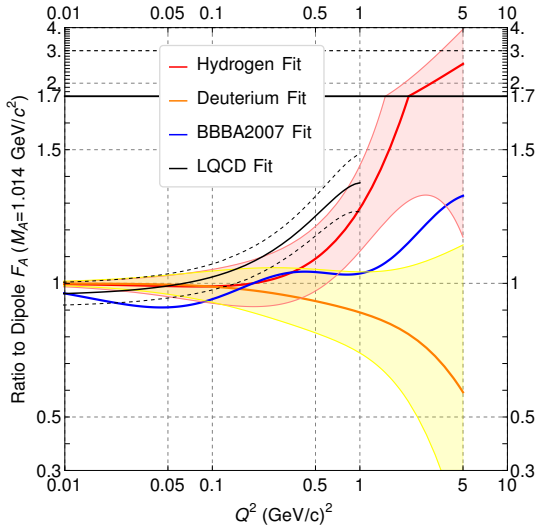

F_{A} fit and axial radius of the nucleon

Result of F_{A} fit:

A fit to lattice QCD calculation by Lin[27] is consistent with our fitted F_{A} up to $1\ (\mathrm{GeV}/c)^2$

LQCD: Lin 2022[27]

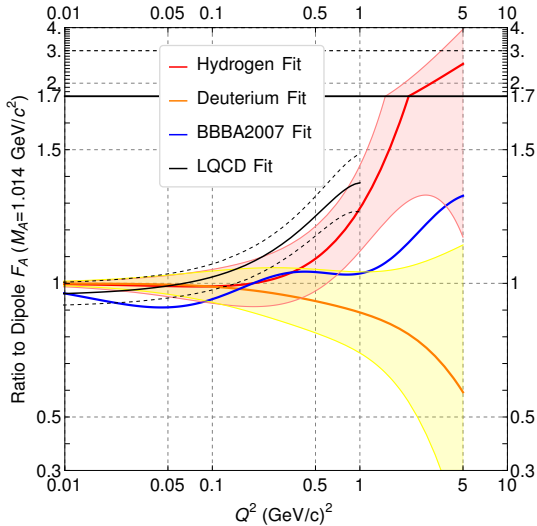

Nucleon form factor impacts DUNE physics

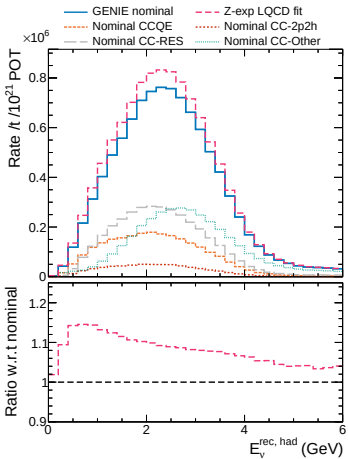

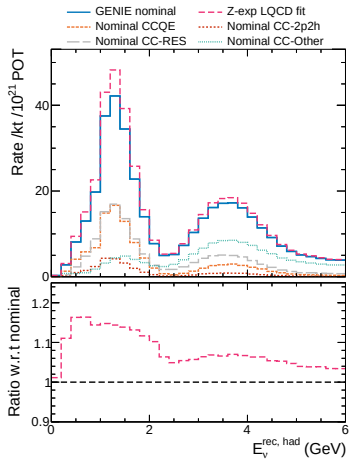

ν_μ event rate in DUNE near (left) and far (right) detector.

$$E_\nu^{\mathrm{rec,had}} = E_l + \sum_p E_{\mathrm{kin}} + \sum_{\pi^\pm,\pi^0,\gamma} E_{\mathrm{tot}}$$

- Solid blue: GENIEv3 10a_02_11a, CCQE uses dipole F_{A}.
- Dashed black: replace dipole F_{A} with z-expansion F_{A} fitted to LatCat LQCD.

$10\% \sim 20\%$ effect.
Meyer, Walker-Loud, and Wilkinson, 2022[28].

Summary

First new nucleon F_{A} measurement in 30 years and the only statistically significant measurement on free nucleon.

- The result will aid in better understanding the weak nucleon structure.
- An important ingredient for DUNE → impacts cross section.
- The new techniques developed are useful for current and future experiments:
  - neutron reconstruction
  - method of background constraint

Appeared online today: *Nature* 614, 48–53 (2023)

Thank you!
The MINERvA Collaboration

Backup

Background constraint method

MC cateogries (**C**) with significant contributions in each Q^2_{QE} bin and angular region is used as template. QELike: CCQE, 2p2h, resonant. Non-QELike: π^0, $\pi^{\pm}$.

$$\chi^2 = \sum_{S,i} \frac{\left(\left[\sum_C w_{C,i} N^{\mathrm{mc}}_{C,S,i}\right] - N^{\mathrm{data}}_{S,i}\right)^2}{N^{\mathrm{data}}_{S,i}} + \qquad \chi^2 \text{ term}$$

$$\lambda_S \sum_C \sum_{j=1}^{N-2} \left(w_{C,j} + w_{C,j+2} - 2w_{C,j+1}\right)^2. \qquad \text{regularizaton term}$$

S: sideband – angular regions participating in fit. **i**: Q^2_{QE} bin. **w**: Weight for each category in each bin.

$\lambda_{\mathbf{S}}$ controls the strength of the regularization, affects smoothness of the fit, and obtained through an L-curve style scan.

Explanation of the Weights

The CCQE weight is affected by

- Base GENIE model
- Various model tunes:
  - RPA, NuWro SF
- Final state tunes:
  - FSI tunes

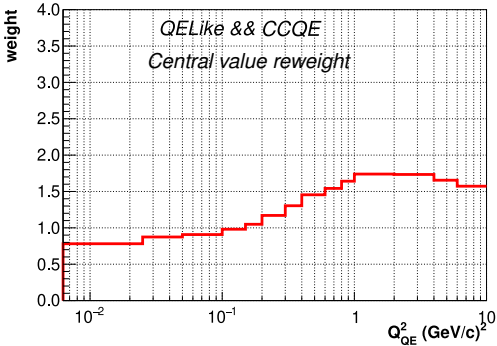

Non-QE **validation region 1** – fitted

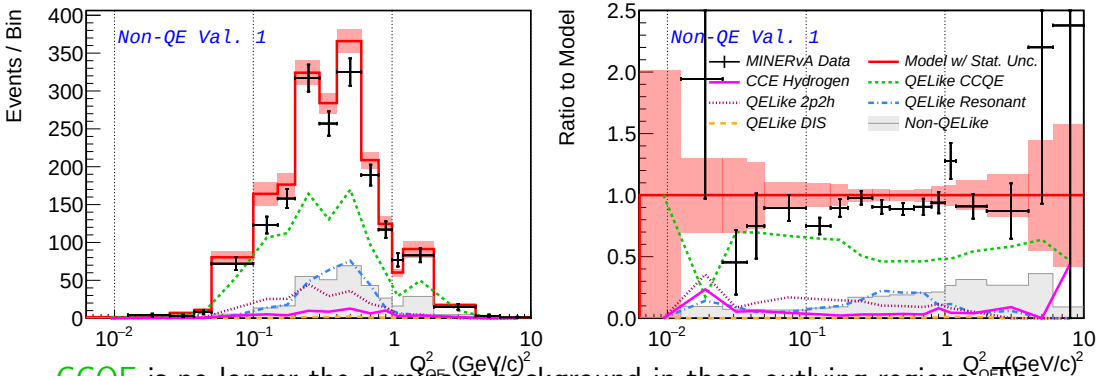

CCQE is no longer the dominant background in these outlying regions. The Non-QE validation regions are mechanically separated into two sub-regions but has smaller effect on the parameter scan due to low statistics.

Non-QE **validation region 2** – fitted

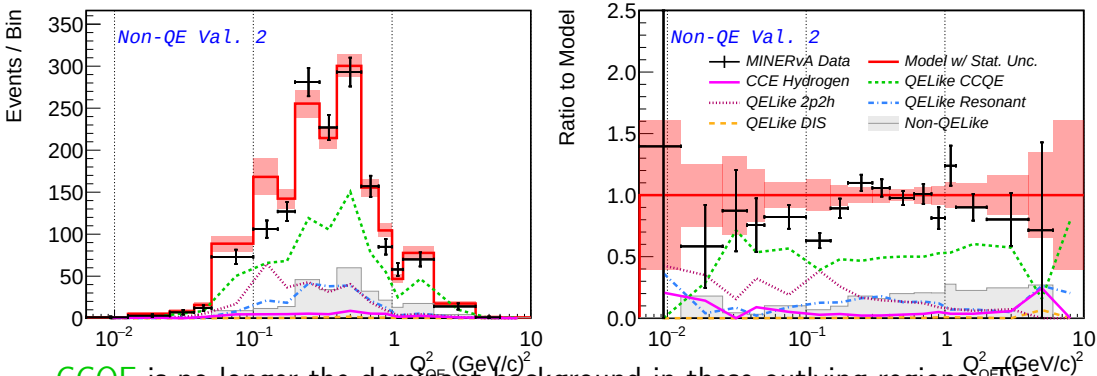

CCQE is no longer the dominant background in these outlying regions. The Non-QE validation regions are mechanically separated into two sub-regions but has smaller effect on the parameter scan due to low statistics.

Non-QE **fit region** – fitted

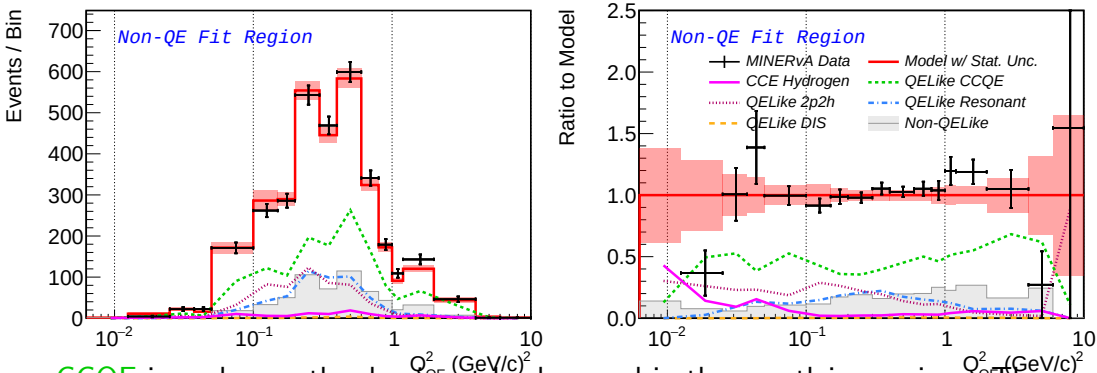

CCQE is no longer the dominant background in these outlying regions. The Non-QE validation regions are mechanically separated into two sub-regions but has smaller effect on the parameter scan due to low statistics.

Non-QE meson **fit region** – fitted

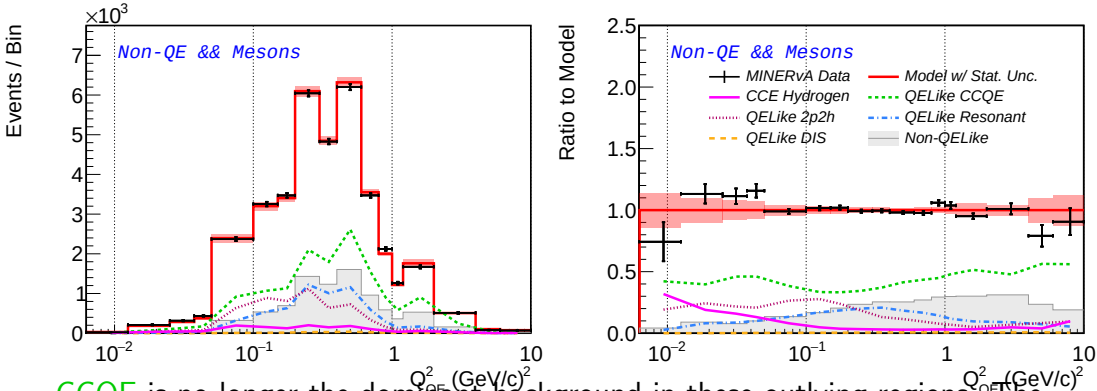

CCQE is no longer the dominant background in these outlying regions. The Non-QE validation regions are mechanically separated into two sub-regions but has smaller effect on the parameter scan due to low statistics.

Effects of background constraint on angular regions

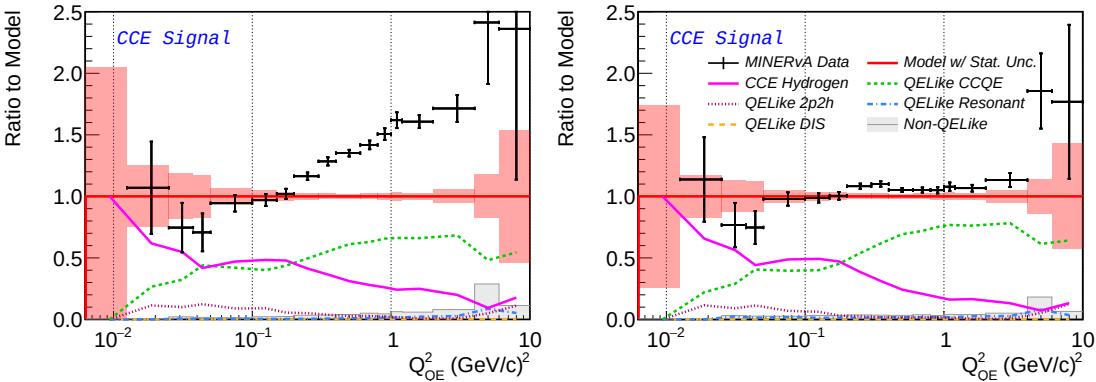

CCE signal region

Ratio of data to (left) unfitted model, (right) post-fitted model.

Effects of background constraint on angular regions

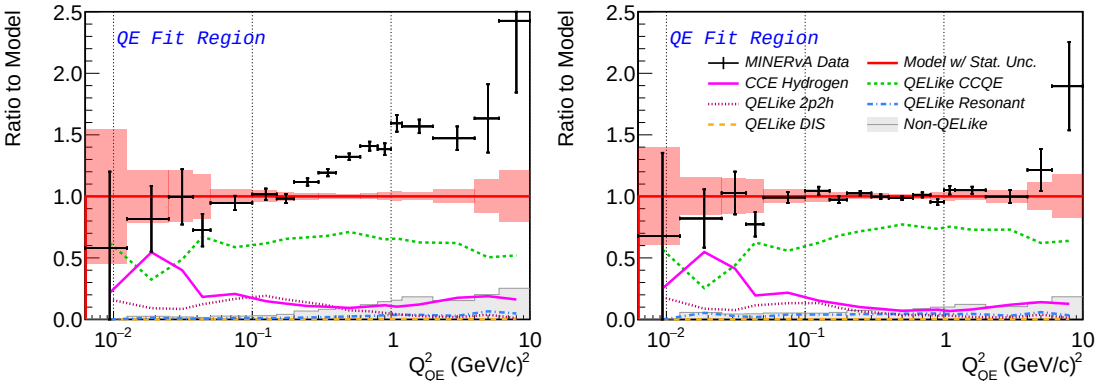

QE fit region

Ratio of data to (left) unfitted model, (right) post-fitted model.

Effects of background constraint on angular regions

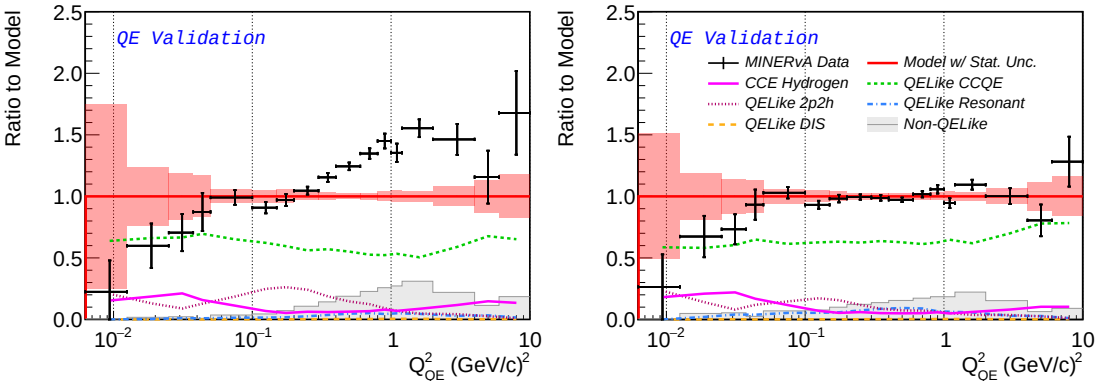

QE validation region

Ratio of data to (left) unfitted model, (right) post-fitted model.

Effects of background constraint on angular regions

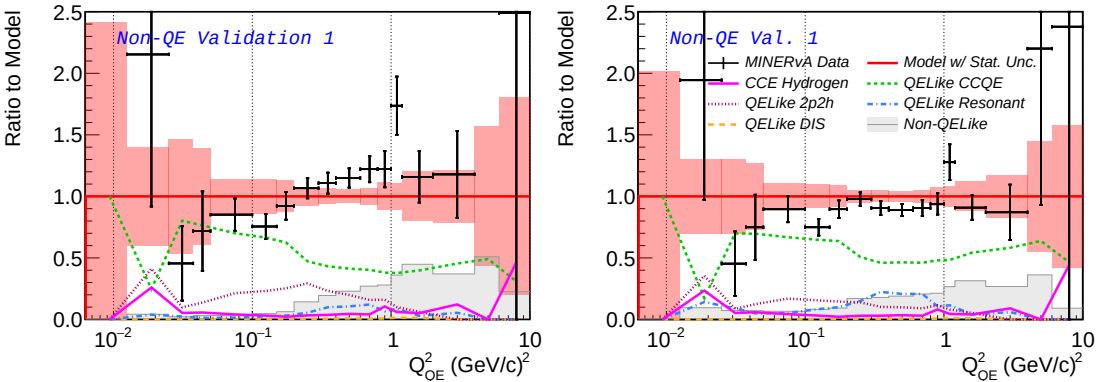

Non-QE validation 1

Ratio of data to (left) unfitted model, (right) post-fitted model.

Effects of background constraint on angular regions

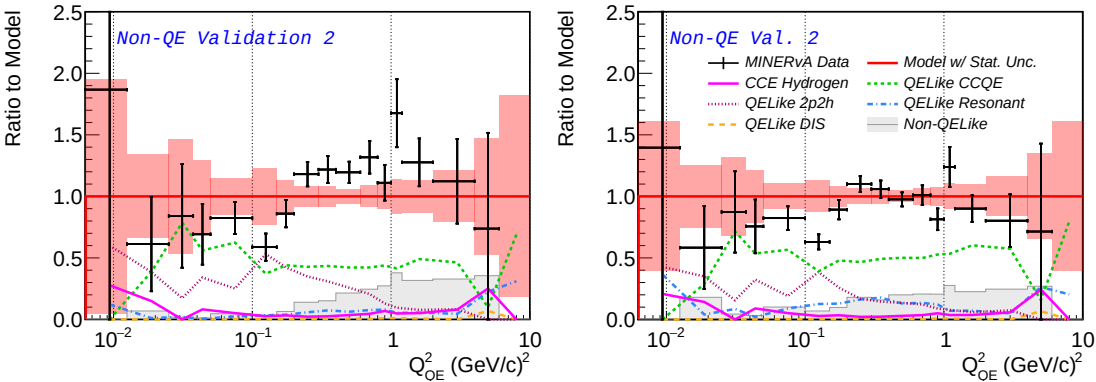

Non-QE validation 2

Ratio of data to (left) unfitted model, (right) post-fitted model.

Effects of background constraint on angular regions

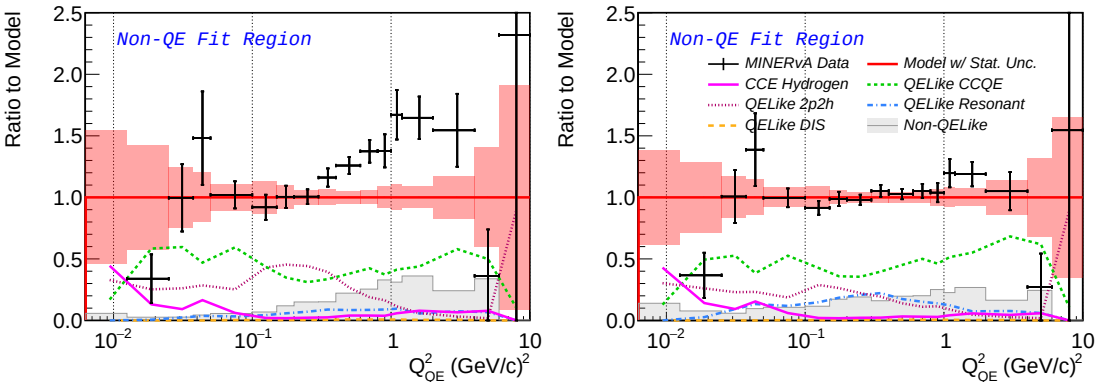

Non-QE fit region

Ratio of data to (left) unfitted model, (right) post-fitted model.

Effects of background constraint on angular regions

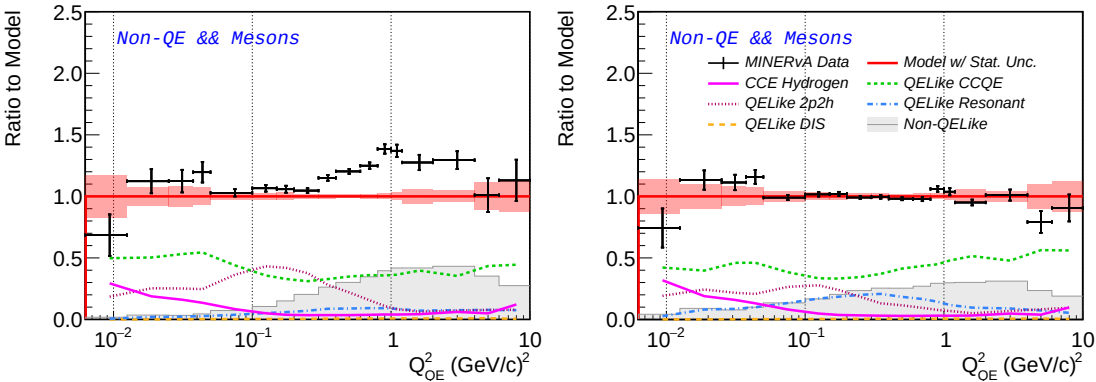

Non-QE and mesons fit region

Ratio of data to (left) unfitted model, (right) post-fitted model.

MINERvA $\bar{\nu}_\mu$-CH result – ratio of data to base model

Bashyal et al., 2022[29]

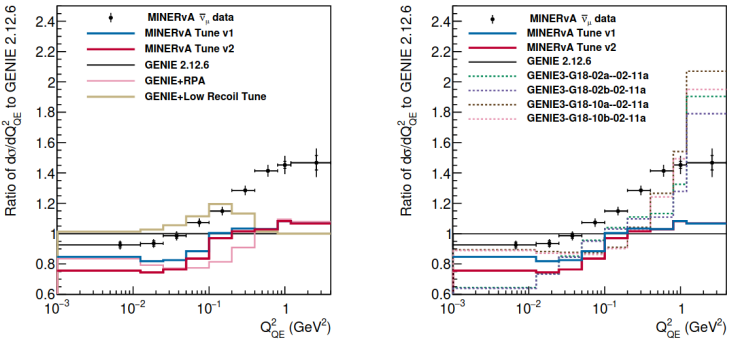

FIG. 4. Comparisons of the cross section predicted by various tunes applied on GENIE with respect to the baseline GENIE 2.12.6 (black) as a function of Q^2_{QE} (left). MINERvA Tune v1 (blue) is the standard simulation tuned to the MINERvA low energy data. MINERvA Tune v2 (red) is MINERvA Tune v1 with the non-resonant pions suppressed in the low Q^2_{QE} region [30]. The remaining curves show the effect of enabling different corrections to the base model. The plots on the right show comparisons of cross sections predictions for GENIE v3.0.6 (dotted lines) with the MINERvA tuned GENIE predictions.Inner ticks in the data are statistical and the outer ticks are the systematic uncertainties.

Migration matrix and warping study

Row normalized migration matrix:
Unfolding matrix obtained by

- D'Agostini iterative unfolding – stops at 4th iteration.

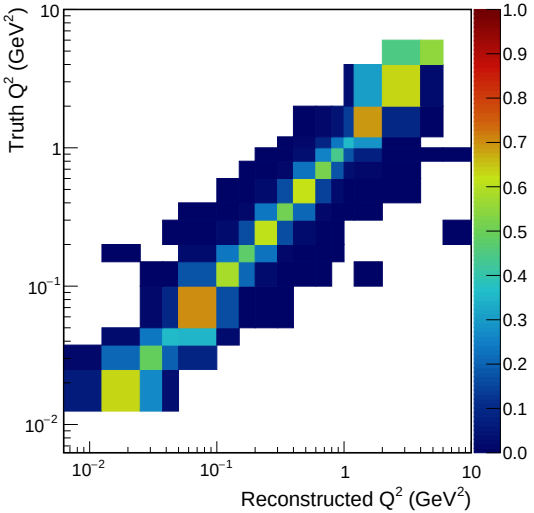

Migration matrix and warping study

Ratio of "warped prediction" to base prediction.

- Performed warping study to check stability of regularization.
- "Warped" prediction with ratio, and
- and generated ensemble of 1000 statistical variations.
- Obtain average and median χ^2 between unfolded and truth of the ensemble for each iteration.

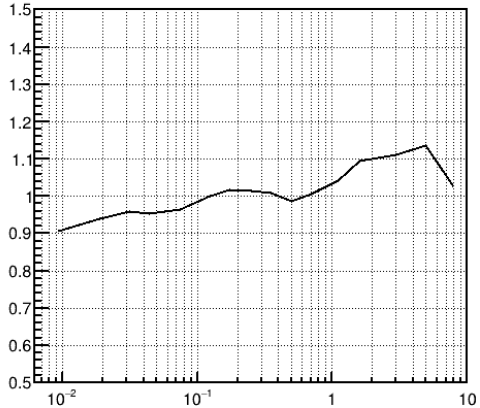

Systematics Uncertainties

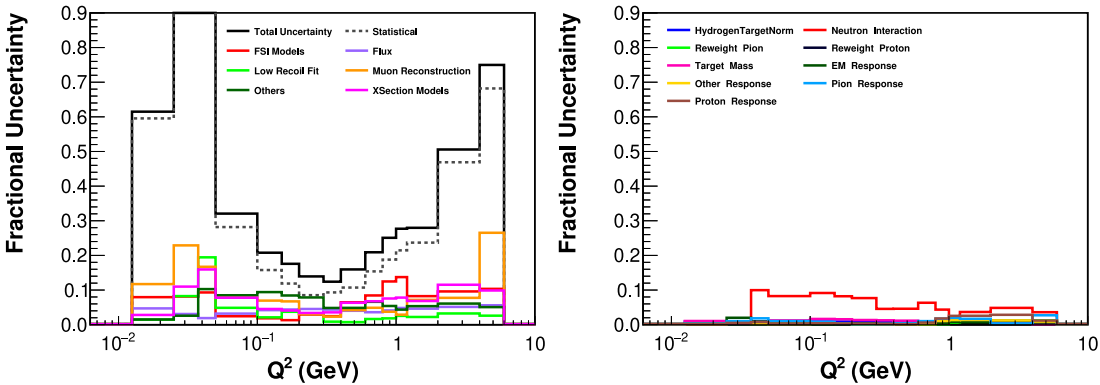

(left) all systematics, (right) others

Systematics Uncertainties

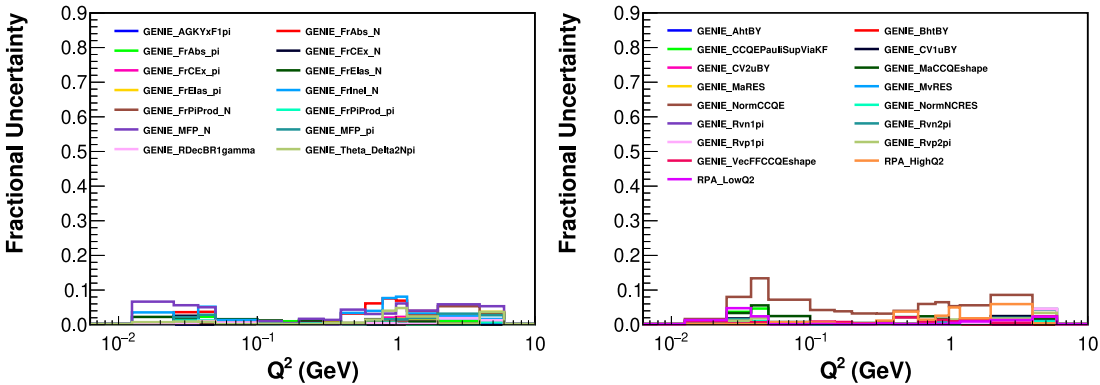

(left) FSI model, (right) cross section model

Systematics Uncertainties

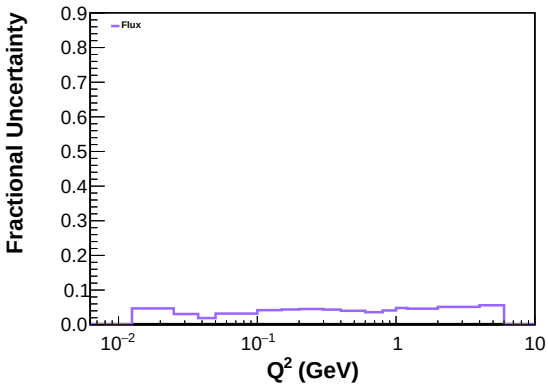

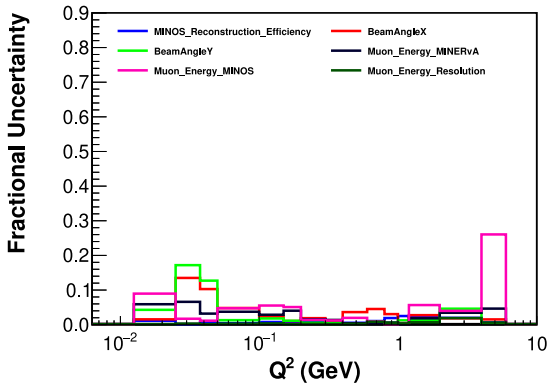

(left) flux, (right) muon reconstruction

Systematics Uncertainties

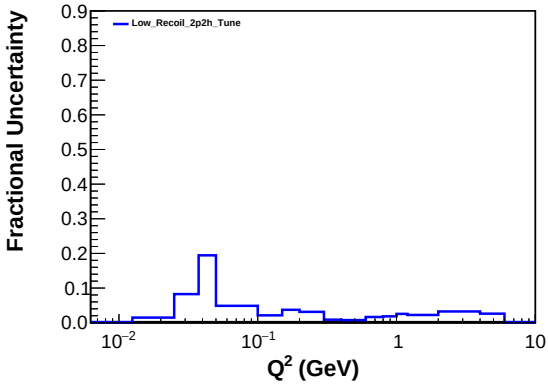

low recoil fit

Neutron secondary scattering

- Ejected protons responsible for majority of secondary neutron interactions.
- Inelastic scattering from carbon dominates (see previous slide)
- MINERνA doesn't have access to the most updated GEANT4 because we need to access MINOS.

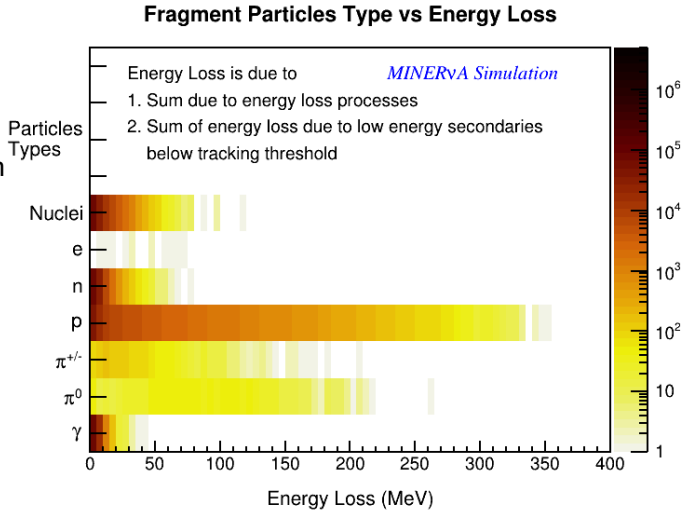

Effect of MONA Reweight – Blob Energy

Without MoNA

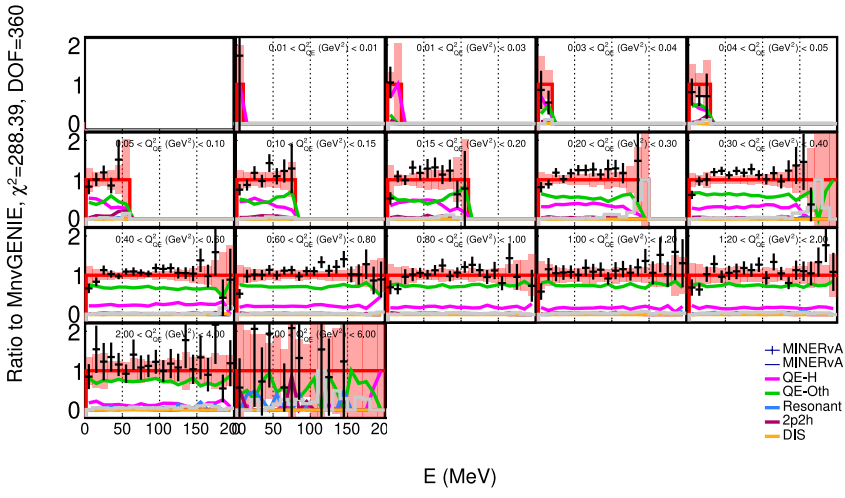

Effect of MONA Reweight – Blob Energy

With MoNA

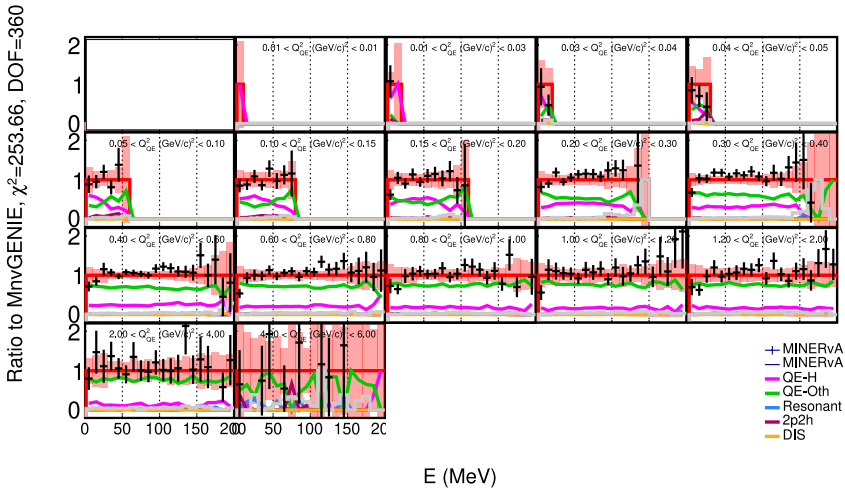

Effect of MONA Reweight – Blob Distance to Vertex

Without MoNA

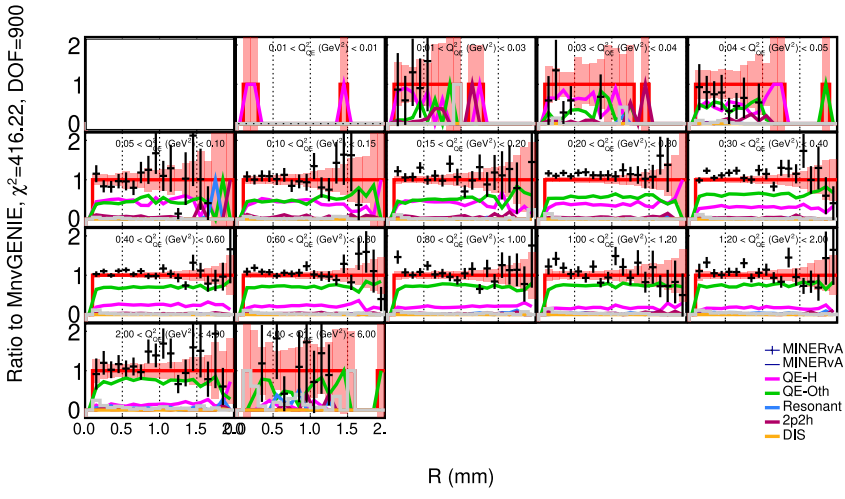

Effect of MONA Reweight – Blob Distance to Vertex

With MoNA

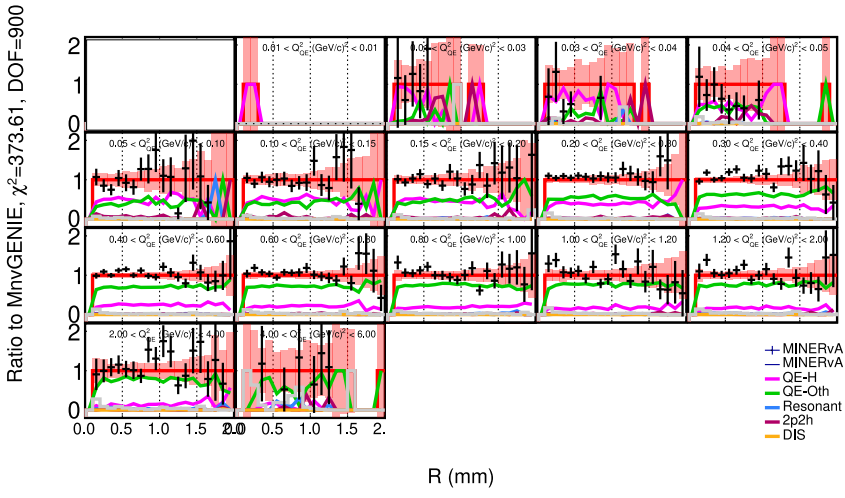

z-expansion parameters

z-expansion formalism and constraints on a_k

$$F_{\mathrm{A}}(Q^2) = \sum_{k=0}^{k_{\max}} a_k z^k$$

$$z = \frac{\sqrt{t_{\mathrm{cut}} + Q^2} - \sqrt{t_{\mathrm{cut}} - t_0}}{\sqrt{t_{\mathrm{cut}} + Q^2} + \sqrt{t_{\mathrm{cut}} - t_0}}$$

$$\sum_{k=n}^{\infty} k(k-1)\dots(k-n+1)a_k = 0, n \in (0,1,2,3)$$

$$\chi^2 = \Delta X \cdot \mathrm{cov}^{-1} \cdot \Delta X + \lambda \left[\sum_{k=1}^{5} \left(\frac{a_k}{5a_0} \right)^2 + \sum_{k=5}^{k_{\max}} \left(\frac{k a_k}{25 a_0} \right)^2 \right]$$

$\Delta X = \mathrm{data} - \mathrm{prediction}$

z-expansion parameters II

Central value fit: $k_{\max} = 8, \lambda = 0.13$

- Scan through large range of λ
- Data χ^2 for $k_{\max} = 8$ can be less than $k_{\max} = 6$
- λ chosen at point of maximum curvature.

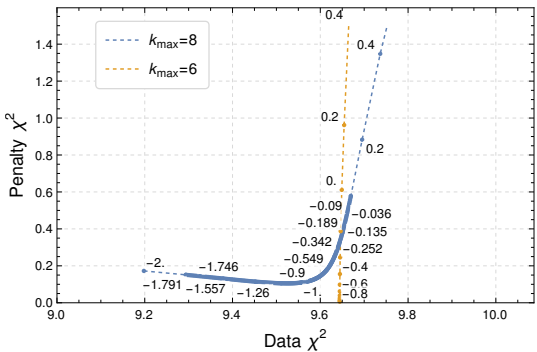

Dipole Fit

- $M_A = 1.15(10)$ GeV
- Fit $\chi^2 = 10.2$
- Comparable with z-expansion fit
  - $k_{\max} = 6$
  - $\lambda = 0$
  - $\chi^2 = 9.64$

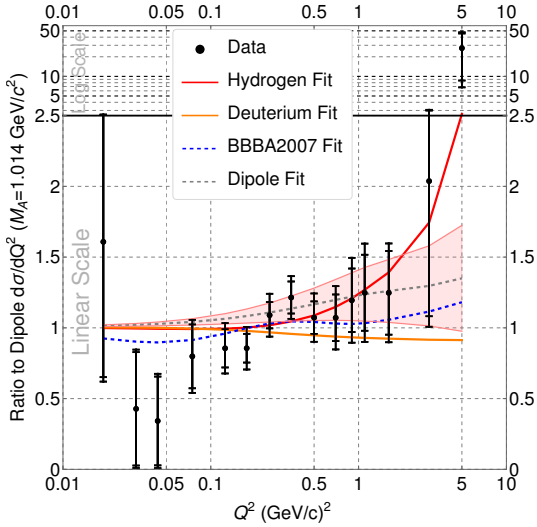

Changing GENIE's initial state model

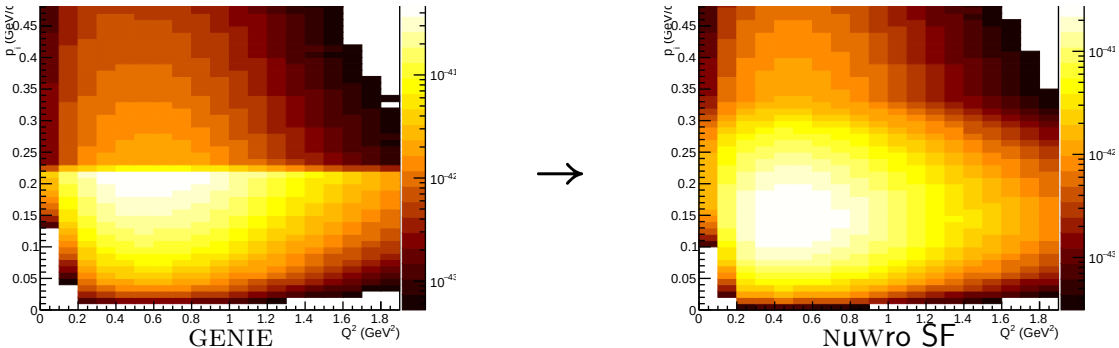

Transform GENIE RFG to NuWro SF
in $|p_i| - Q^2$ space

Relativistic Fermi Gas (RFG), Local Fermi Gas (LFG) and Spectral Function (SF)

- RFG: non-interacting fermions in a potential well with fixed Fermi momentum K_F.
- GENIE RFG includes an additional tail.
- LFG: Fermi gas with location-dependent K_F.
- SF: a nuclear-shell model.

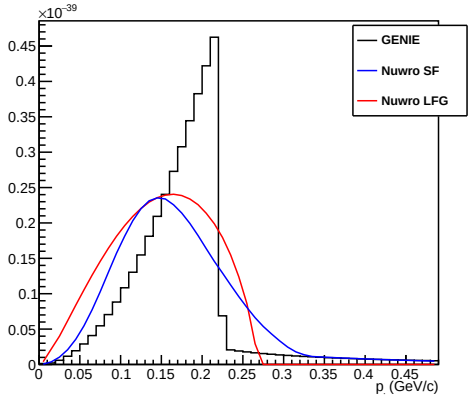

Initial state momentum distribution.

F_A fit and axial radius of the nucleon

Favors larger F_A at higher Q^2.
Calculate proton radius from F_A for $Q^2 \to 0$.

$$F_A(Q^2) = F_A(0)\left(1 - \frac{\langle r_A^2\rangle}{3!}Q^2 + \frac{\langle r_A^4\rangle}{5!}Q^4 + \dots\right),$$

$$\frac{1}{F_A(0)}\frac{dF_A}{dQ^2}\bigg|_{Q^2=0} = -\frac{1}{6}\langle {r_A}^2\rangle$$

- $\langle r_A^2\rangle = 0.53(25)\text{fm}^2$
- $\sqrt{\langle r_A^2\rangle} = 0.73(17)\text{fm}$

Deuterium Fit[25], BBBA2007[26], LQCD[27]

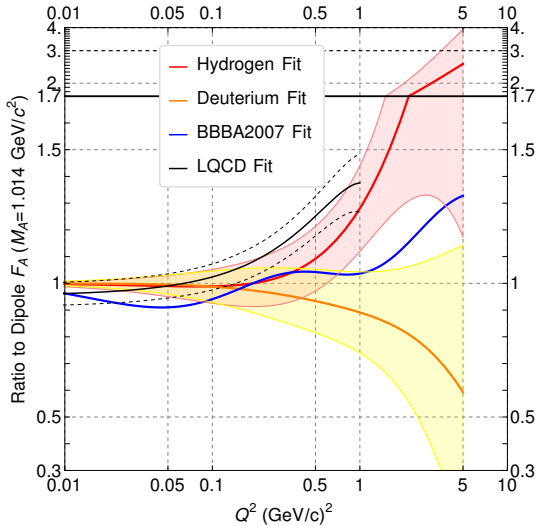

Deuterium Fit[25], BBBA2007[26], LQCD[27]

F_{A} fit and axial radius of the nucleon

Favors larger F_{A} at higher Q^2.
Calculate proton radius from F_{A} for $Q^2 \to 0$.

$$F_{\mathrm{A}}(Q^2) = F_{\mathrm{A}}(0)\left(1 - \frac{\langle r_A^2\rangle}{3!}Q^2 + \frac{\langle r_A^4\rangle}{5!}Q^4 + \dots\right),$$

$$\frac{1}{F_{\mathrm{A}}(0)}\frac{\mathrm{d}F_{\mathrm{A}}}{\mathrm{d}Q^2}\bigg|_{Q^2=0} = -\frac{1}{6}\langle {r_A}^2\rangle$$

- $\langle r_A^2\rangle = 0.53(25)\mathrm{fm}^2$
- $\sqrt{\langle r_A^2\rangle} = 0.73(17)\mathrm{fm}$

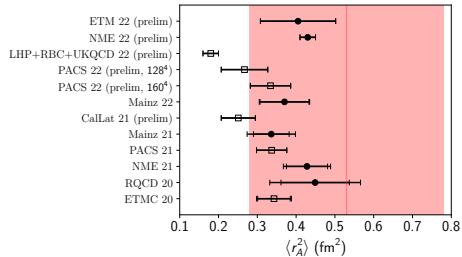

Filled circle: full error budget.
Open square: incomplete.
Red band: this result.
Courtesy of Aaron Meyer.

Reference

Reference I

[1] J. A. Formaggio and G. P. Zeller. "From eV to EeV: Neutrino cross sections across energy scales". In: *Rev. Mod. Phys.* 84 (3 Sept. 2012), pp. 1307–1341. DOI: 10.1103/RevModPhys.84.1307. URL: https://link.aps.org/doi/10.1103/RevModPhys.84.1307.

[2] C. H. Llewellyn Smith. "Neutrino Reactions at Accelerator Energies". In: *Phys. Rept.* 3 (1972), pp. 261–379. DOI: 10.1016/0370-1573(72)90010-5.

[3] K.A. Olive. "Review of Particle Physics". In: *Chinese Physics C* 40.10 (Oct. 2016), p. 100001. DOI: 10.1088/1674-1137/40/10/100001. URL: https://doi.org/10.1088/1674-1137/40/10/100001.

Reference II

[4] G. Fanourakis et al. "Study of low-energy antineutrino interactions on protons". In: *Phys. Rev. D* 21 (3 Feb. 1980), pp. 562–568. DOI: 10.1103/PhysRevD.21.562. URL: https://link.aps.org/doi/10.1103/PhysRevD.21.562.

[5] W. A. Mann et al. "Study of the reaction nu n —> mu- p". In: *Phys. Rev. Lett.* 31 (1973), pp. 844–847. DOI: 10.1103/PhysRevLett.31.844.

[6] A. A. Aguilar-Arevalo et al. "First Measurement of the Muon Neutrino Charged Current Quasielastic Double Differential Cross Section". In: *Phys. Rev. D* 81 (2010), p. 092005. DOI: 10.1103/PhysRevD.81.092005. arXiv: 1002.2680 [hep-ex].

Reference III

[7] A. V. Butkevich and D. Perevalov. "Determination of the Axial Nucleon Form Factor from the MiniBooNE Data". In: *Phys. Rev. D* 89.5 (2014), p. 053014. DOI: 10.1103/PhysRevD.89.053014. arXiv: 1311.3754 [hep-ph].

[8] G. A. Fiorentini et al. "Measurement of Muon Neutrino Quasielastic Scattering on a Hydrocarbon Target at $E_\nu \sim 3.5$ GeV". In: *Phys. Rev. Lett.* 111 (2013), p. 022502. DOI: 10.1103/PhysRevLett.111.022502. arXiv: 1305.2243 [hep-ex].

[9] D. Ruterbories et al. "Simultaneous Measurement of Proton and Lepton Kinematics in Quasielasticlike $\nu\mu$-Hydrocarbon Interactions from 2 to 20 GeV". In: *Phys. Rev. Lett.* 129.2 (2022), p. 021803. DOI: 10.1103/PhysRevLett.129.021803. arXiv: 2203.08022 [hep-ex].

Reference IV

[10] J. Kleykamp et al. "Simultaneous measurement of muon neutrino quasielastic-like cross sections on CH, C, water, Fe, and Pb as a function of muon kinematics at MINERvA". In: (Jan. 2023). arXiv: 2301.02272 [hep-ex].

[11] Matteo Vicenzi. "SAND - System for on-Axis Neutrino Detection - in the DUNE Near Detector Complex". In: *PoS* NuFact2021 (2022), p. 248. DOI: 10.22323/1.402.0248.

[12] L. Zazueta et al. "Improved constraint on the MINERvA medium energy neutrino flux using $\bar{\nu}e^- \to \bar{\nu}e^-$ data". In: (Sept. 2022). arXiv: 2209.05540 [hep-ex].

[13] J. Nieves, I. Ruiz Simo, and M. J. Vicente Vacas. "Inclusive Charged–Current Neutrino–Nucleus Reactions". In: *Phys. Rev.* C83 (2011), p. 045501. DOI: 10.1103/PhysRevC.83.045501. arXiv: 1102.2777 [hep-ph].

Reference V

[14] P. A. Rodrigues, J. Demgen, E Miltenberger, et al. "Identification of Nuclear Effects in Neutrino-Carbon Interactions at Low Three-Momentum Transfer". In: *Phys. Rev. Lett.* 116 (7 Feb. 2016), p. 071802. DOI: 10.1103/PhysRevLett.116.071802. URL: https://link.aps.org/doi/10.1103/PhysRevLett.116.071802.

[15] J. Nieves, Jose Enrique Amaro, and M. Valverde. "Inclusive quasi-elastic neutrino reactions". In: *Phys. Rev.* C70 (2004). [Erratum: Phys. Rev.C72,019902 p. 055503. DOI: 10.1103/PhysRevC.70.055503,10.1103/PhysRevC.72.019902. arXiv: nucl-th/0408005 [nucl-th].

Reference VI

[16] Philip Rodrigues, Callum Wilkinson, and Kevin McFarland. "Constraining the GENIE model of neutrino-induced single pion production using reanalyzed bubble chamber data". In: *Eur. Phys. J.* C76.8 (2016), p. 474. DOI: 10.1140/epjc/s10052-016-4314-3. arXiv: 1601.01888 [hep-ex].

[17] P. Stowell et al. "Tuning the genie pion production model with MINERvA data". In: *Physical Review D* 100.7 (Oct. 2019). ISSN: 2470-0029. DOI: 10.1103/physrevd.100.072005. URL: http://dx.doi.org/10.1103/PhysRevD.100.072005.

[18] L. A. Harewood and R. Gran. "Elastic hadron-nucleus scattering in neutrino-nucl reactions and transverse kinematics measurements". In: (2019). arXiv: 1906.10576 [hep-ex].

Reference VII

[19] Artur M. Ankowski and Jan T. Sobczyk. "Construction of spectral functions for medium-mass nuclei". In: *Phys. Rev.* C77 (2008), p. 044311. DOI: 10.1103/PhysRevC.77.044311. arXiv: 0711.2031 [nucl-th].

[20] C. Juszczak, J. A. Nowak, and J. T. Sobczyk. "Spectrum of recoil nucleons in quasi-elastic neutrino nucleus interactions". In: *Eur. Phys. J. C* 39 (2005), pp. 195–200. DOI: 10.1140/epjc/s2004-02086-9.

[21] A. Del Guerra. "A compilation of n-p and n-C cross sections and their use in a Monte Carlo program to calculate the neutron detection efficiency in plastic scintillator in the energy range 1–300 MeV". In: *Nuclear Instruments and Methods* 135.2 (1976), pp. 337–352. ISSN: 0029-554X. DOI: https://doi.org/10.1016/0029-554X(76)90181-6. URL: https://www.sciencedirect.com/science/article/pii/0029554X76901816.

Reference VIII

[22] Z. Kohley et al. "Modeling interactions of intermediate-energy neutrons in a plastic scintillator array with Geant4". In: *Nuclear Instruments and Methods in Physics Research Section A: Accelerators, Spectrometers, Detectors and Associated Equipment* 682 (2012), pp. 59–65. ISSN: 0168-9002. DOI: https://doi.org/10.1016/j.nima.2012.04.060. URL: https://www.sciencedirect.com/science/article/pii/S0168900212004329.

[23] T. Cai et al. "Nucleon binding energy and transverse momentum imbalance in neutrino-nucleus reactions". In: *Phys. Rev. D* 101.9 (2020), p. 092001. DOI: 10.1103/PhysRevD.101.092001. arXiv: 1910.08658 [hep-ex].

Reference IX

[24] R. Bradford et al. "A New parameterization of the nucleon elastic form-factors". In: *Nucl. Phys. B Proc. Suppl.* 159 (2006). Ed. by F. Cavanna, J. G. Morfin, and T. Nakaya, pp. 127–132. DOI: 10.1016/j.nuclphysbps.2006.08.028. arXiv: hep-ex/0602017.

[25] Aaron S. Meyer et al. "Deuterium target data for precision neutrino-nucleus cross sections". In: *Phys. Rev. D* 93.11 (2016), p. 113015. DOI: 10.1103/PhysRevD.93.113015. arXiv: 1603.03048 [hep-ph].

[26] A. Bodek et al. "Vector and Axial Nucleon Form Factors:A Duality Constrained Parameterization". In: *Eur. Phys. J. C* 53 (2008), pp. 349–354. DOI: 10.1140/epjc/s10052-007-0491-4. arXiv: 0708.1946 [hep-ex].

Reference X

[27] Huey-Wen Lin. "Nucleon helicity generalized parton distribution at physical pion mass from lattice QCD". In: *Phys. Lett. B* 824 (2022), p. 136821. DOI: 10.1016/j.physletb.2021.136821. arXiv: 2112.07519 [hep-lat].

[28] Aaron S. Meyer, André Walker-Loud, and Callum Wilkinson. "Status of Lattice QCD Determination of Nucleon Form Factors and their Relevance for the Few-GeV Neutrino Program". In: (Jan. 2022). DOI: 10.1146/annurev-nucl-010622-120608. arXiv: 2201.01839 [hep-lat].

[29] A. Bashyal et al. "High-Statistics Measurement of Antineutrino Quasielastic-like scattering at $E_\nu \sim 6$˜GeV on a Hydrocarbon Target". In: (Nov. 2022). arXiv: 2211.10402 [hep-ex].